

Potential Black Hole Seeding of the Spiral Galaxy NGC 4424 via an Infalling Star Cluster

ALISTER W. GRAHAM,¹ ROBERTO SORIA,^{2,3} BOGDAN C. CIAMBUR,^{4,5} BENJAMIN L. DAVIS,^{1,6} AND DOUGLAS A. SWARTZ⁷

¹*Centre for Astrophysics and Supercomputing, Swinburne University of Technology, Victoria 3122, Australia*

²*College of Astronomy and Space Sciences, University of the Chinese Academy of Sciences, Beijing 100049, China*

³*Sydney Institute for Astronomy, School of Physics A28, The University of Sydney, Sydney, NSW 2006, Australia*

⁴*LERMA, Observatoire de Paris, CNRS, PSL University, Sorbonne Universités, UPMC Univ. Paris 06, F-75014 Paris, France*

⁵*GEPI, Observatoire de Paris, PSL Research University, Place Jules Janssen, F-92190 Meudon, France*

⁶*Center for Astro, Particle, and Planetary Physics (CAP³), New York University Abu Dhabi, United Arab Emirates*

⁷*Astrophysics Office, NASA Marshall Space Flight Center, ZP12, Huntsville, AL 35812, USA*

ABSTRACT

Galaxies can grow through their mutual gravitational attraction and subsequent union. While orbiting a regular high-surface-brightness galaxy, the body of a low-mass galaxy can be stripped away. However, the stellar heart of the infalling galaxy, if represented by a tightly bound nuclear star cluster, is more resilient. From archival Hubble Space Telescope images, we have discovered a red, tidally-stretched star cluster positioned $\sim 5''$ (~ 400 pc in projection) from, and pointing toward the center of, the post-merger spiral galaxy NGC 4424. The star cluster, which we refer to as ‘Nikhuli’, has a near-infrared luminosity of $(6.88 \pm 1.85) \times 10^6 L_{\odot, F160W}$ and likely represents the nucleus of a captured/wedded galaxy. Moreover, from our Chandra X-ray Observatory image, Nikhuli is seen to contain a high-energy X-ray point source, with $L_{0.5-8 \text{ keV}} = 6.31^{+7.50}_{-3.77} \times 10^{38} \text{ erg s}^{-1}$ (90% confidence). We argue that this is more likely to be an active massive black hole than an X-ray binary. Lacking an outward-pointing comet-like appearance, the stellar structure of Nikhuli favors infall rather than the ejection from a gravitational-wave recoil event. A minor merger with a low-mass early-type galaxy may have sown a massive black hole, aided an X-shaped pseudobulge, and be sewing a small bulge. The stellar mass and the velocity dispersion of NGC 4424 predict a central black hole of $(0.6-1.0) \times 10^5 M_{\odot}$, similar to the expected intermediate-mass black hole in Nikhuli, and suggestive of a black hole supply mechanism for bulgeless late-type galaxies. We may potentially be witnessing black hole seeding by capture and sinking, with a nuclear star cluster the delivery vehicle.

1. INTRODUCTION

Galaxies have long been known to merge. Smaller galaxies rain down on bigger galaxies, stoking their growth (Lindblad 1927; Spitzer & Baade 1951; Baade & Minkowski 1954; Vorontsov-Vel’Yaminov 1959; Ibata et al. 2019b). This evolution has become a defining tenet of the cold dark matter model. The ongoing discovery of (infalling) satellites continues to test and support the hierarchical growth scenario for galaxies. The burgeoning detection of drawn-out, low surface brightness, debris streams of former galaxies in the outskirts of larger galaxies (Putman et al. 1998; Belokurov et al. 2006; Martin et al. 2014; Drlica-Wagner et al. 2015; Koposov et al. 2015; Shipp et al. 2018; Martinez-Delgado et al. 2021) are starting to reveal the extent of the hi-

erarchical model, at least in regard to building stellar halos. The closest known tidal stream to the center of our galaxy is 10-20 kpc distant from the galaxy center (Yuan et al. 2020; Malhan et al. 2021).

The dense and compact nuclear star clusters—which are common features at the centers of low ($\approx 10^7-10^9 M_{\odot}$) and intermediate stellar mass ($\approx 10^9-10^{10.5} M_{\odot}$) galaxies (e.g. Sandage et al. 1985; Böker et al. 2002; Graham & Guzmán 2003; Balcells et al. 2003, 2007; Scott & Graham 2013; Sánchez-Janssen et al. 2019)—are more strongly gravitationally bound than their host galaxies and are thus more able to resist disruption during the cannibalistic process (e.g., Bekki et al. 2001, 2003). Indeed, the dual and multiple nuclei of massive early-type galaxies is a testament to the robustness of these captured star clusters during the galaxy assimilation process (e.g., Jenner 1974; Petrosian et al. 1978; Korovnikovskii et al. 1981; Tonry 1985; Blakeslee & Tonry 1992; Bonfini & Graham 2016).

Furthermore, the abundance of kinematically distinct cores and nuclear stellar disks in early-type galaxies (e.g. [Franx et al. 1989](#); [Forbes et al. 1995](#); [Graham et al. 1998](#); [Hau et al. 1999](#)) reveals a more complete journey to the center of these galaxies, in stark contrast with an eternity spent in the halo.

Such galaxy growth, revealed by off-center nuclei, can be harder to spot in late-type galaxies due to confusion with knots of star formation. This ambiguity makes the later stages of the merger/digestion process more challenging to establish in late-type galaxies. Furthermore, without a massive stellar bulge, dynamical friction will be less in the inner regions, reducing the extent to which minor mergers contribute to the nuclei and bulges. The abundance of low bulge-to-total stellar mass ratios in late-type galaxies identified by [Graham & Worley \(2008\)](#) and [Weinzirl et al. \(2009\)](#) was later used by [Kormendy et al. \(2010\)](#) to challenge the hierarchical growth of most late-type galaxies. It was speculated that the bulges were too small to be built by mergers and were thus considered the result of internal secular processes. The detection of an infalling nuclear star cluster near the center of a late-type spiral galaxy would reveal that the Roche-lobe destruction of galactic neighbors does not just produce streams that build diffuse halos, but that tidal-shredding also contributes to the galaxy proper, including small bulges. Moreover, such digestion could potentially seed and feed spiral galaxies with massive black holes.

Among the Virgo cluster’s spiral galaxies, the ‘Sa? pec’ ([Sandage & Tammann 1981](#)) galaxy NGC 4424 (VCC 979), with a disk-inclination of 70deg from face-on, is of particular interest. While there is no detectable X-ray point source at the center of NGC 4424, there is a nearby ($\sim 5''$) ‘off-center’ source, NGC 4424 X-3 ($L_{0.5-8\text{ keV}} \approx 6 \times 10^{38} \text{ erg s}^{-1}$). First publicly reported by [Boselli et al. \(2018\)](#), they suggested it is either an X-ray binary (XRB) or the nucleus of a merged galaxy. Two brighter X-ray point sources plus a fainter fourth point source reside in the outskirts of this galaxy.

Although [Feng & Soria \(2011\)](#), [Bachetti et al. \(2014\)](#) and [Kaaret et al. \(2017\)](#) reveal why super-Eddington accretion ([Alexander & Natarajan 2014](#); [Soria et al. 2014](#)) is thought to explain many of the off-center ultraluminous X-ray sources (ULX: $L_X \approx 3 \times 10^{39}$ to $10^{41} \text{ erg s}^{-1}$), some might be intermediate-mass black holes (IMBHs) from accreted galaxies, particularly the hyperluminous X-ray sources (HLXs: $L_X > 10^{41} \text{ erg s}^{-1}$, [Gao et al. 2003](#)) such as ESO 243-49 ([Farrell et al. 2009](#); [Soria et al. 2010](#)) and others ([Sutton et al. 2012](#); [Barrows et al. 2019](#); [Earnshaw et al. 2019](#)). Here, we report the association of NGC 4424 X-3 with a red, elongated star cluster.

In Section 2, we provide some background information and references to NGC 4424 before presenting optical and near-infrared images along with an X-ray map. We perform a re-analysis of the Hubble Space Telescope (HST) image, the Chandra X-ray Observatory (CXO) and XMM-Newton data, and provide an extended discussion. Section 3 offers a prediction for the mass of the central black hole in both NGC 4424 and the suspected infaller. Finally, a more detailed discussion, centered around off-centered sources, is provided in Section 5.

Previously, in [Graham et al. \(2019\)](#), we used the mean redshift-independent distance modulus for NGC 4424 of 30.6 ± 1.0 from the NASA/IPAC Extragalactic Database (NED)¹. Here, we adopt the Cepheid-based distance modulus of 31.080 ± 0.292 (luminosity distance $D = 16.44^{+2.37}_{-2.07} \text{ Mpc}$) from [Riess et al. \(2016\)](#), giving a scale of 79 pc arcsec⁻¹. This encompasses and agrees with an array of recent results, including [Hatt et al. \(2018\)](#), who report a ‘tip of the red giant branch’ distance modulus of $31.00 \pm 0.03_{\text{stat}} \pm 0.06_{\text{sys}}$ ($15.8 \pm 0.2_{\text{stat}} \pm 0.4_{\text{sys}} \text{ Mpc}$), and with [Munari et al. \(2013\)](#), who derived a SN Ia distance modulus of 30.95, and with [Cortés et al. \(2008\)](#), who reported a value of 30.91 based on the [Tully & Fisher \(1977\)](#) relation.

2. OBSERVATIONS AND FINDINGS

2.1. Preface

From deep CXO exposures of 100 early-type galaxies in the Virgo cluster—half of which possess a nuclear star cluster ([Côté et al. 2006](#); [Ferrarese et al. 2006](#))—[Gallo et al. \(2010\)](#) effectively reveals that nuclear star clusters, in and of themselves, tend not to contain X-ray point sources. Among the 30 lowest mass galaxies of that 100-strong sample, most are nucleated, and all have been predicted to harbour an IMBH. [Graham & Soria \(2019\)](#) reported that just three of these 30 contained a central X-ray point source, ruling out stellar-mass XRBs as a common feature of nuclear star clusters, at least in early-type galaxies. If these star clusters are comprised of both a young and old stellar population, it will rule out both high- and low-mass XRBs, respectively.

From past observations, NGC 4424 (Figure 1) has been identified as a post-merger galaxy experiencing central star formation ([Kenney et al. 1996](#)). [Cortés et al. \(2006\)](#) and [Boselli et al. \(2018\)](#) provide a detailed analysis of NGC 4424, finding that it experienced an unequal-mass merger event less than 0.5 Gyr ago. The encounter has fueled an outburst of ionized gas, evident as a $\sim 10 \text{ kpc}$ plume pointing in the opposite direction

¹ <http://nedwww.ipac.caltech.edu>

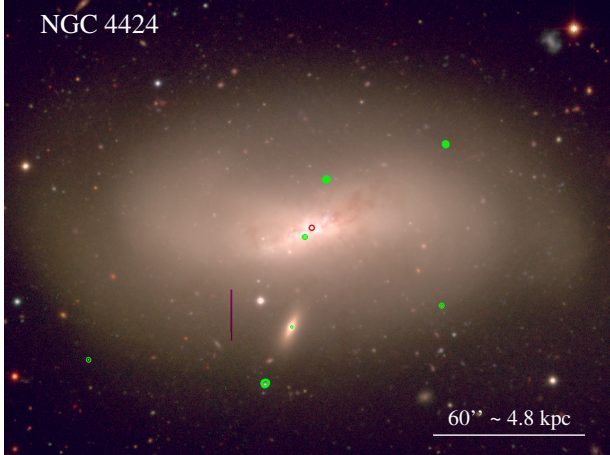


Figure 1. Next Generation Virgo Cluster Survey (NGVS: Ferrarese et al. 2012) image of the post-merger galaxy NGC 4424 (red = i filter; green = g ; blue = u), with CXO/ACIS-S contours (0.5–7.0 keV band) overlaid in green. North is up, east is to the left. The red circle shows the NED-provided position for the galaxy’s optical nucleus, with a radius of 1 arcsec capturing the associated uncertainty. The near-central, but off-center, X-ray point source (NGC 4424 X-3) is associated with an elongated star cluster (see Figures 2 and 3). The galaxy to the south is IC 3366 (LEDA 213994), a background galaxy at a distance of ~ 110 Mpc, while the vertical red stripe is an artifact that should be ignored.

to a ~ 110 kpc long (ram pressure)-stripped tail of HI gas emanating from NGC 4424 as it plows through the hot intracluster medium of the Virgo cluster.

2.2. Optical/near-IR images

From Figure 1, obtained as a part of the Next Generation Virgo Cluster Survey (NGVS: Ferrarese et al. 2012), NGC 4424 appears as a bulgeless, or near-bulgeless, galaxy containing a knotty bar-like feature with an ellipticity to great to be a (relaxed) bulge. While de Vaucouleurs et al. (1991) catalog this galaxy as having spiral arms and a bar, this bar-like feature does not resemble a typical (relaxed) bar. Instead, it displays an apparent X/(peanut shell)-shaped (X/P) structure; a pseudobulge formed from the buckling of a bar (Bardeen 1975; Hohl 1975; Combes & Sanders 1981; Combes et al. 1990; Athanassoula 2005; Saha et al. 2018). The broad, faint spiral arms emanate from the ends of the X-shaped bar-like feature, at a major-axis radius of $\sim 36''$.

Zooming in on the central region, and dialing down the brightness, Figure 2 shows part of an image acquired from the Hubble Legacy Archive (HLA)². It displays

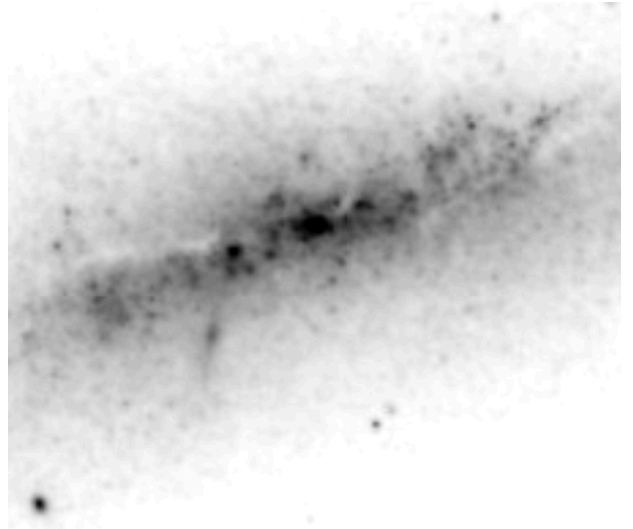


Figure 2. *HST*/WFC3-IR F160W image of the inner $21'' \times 18''$ region of NGC 4424, displaying an elongated arc or stream with a nucleus $5''$ to the southeast of the galaxy center. The near-central X-ray point-source in Figure 1 coincides with this nucleus. North is up, east is to the left. Image: HLA Dataset hst_12880_26_wfc3_ir_f160w.

the inner region of a Wide Field Camera 3 (WFC3) IR channel F160W (H -band) image taken as a part of *HST* Proposal ID 12880 (PI: A.Riess). The near-IR exposure helps to reduce the impact of dust, young stars and avoid $H\alpha$ emission. One can see a nucleated stream to the lower-left (southeast) of the galaxy center.

Figure 3 shows our modeling and removal of much of the galaxy’s mirror-symmetric light about its major-axis (having a variable position angle with radius). Our data reduction process followed that detailed in Davis et al. (2019). We modeled NGC 4424 using the modified task *Isofit* (Ciambur 2015), run within the Image Reduction and Analysis Facility (IRAF)³ package ELLIPSE. Our model consists of a series of one-dimensional profiles including the radial run of intensity, major-axis position angle, ellipticity and a sequence of higher-order Fourier harmonic terms capturing the isophotes’ departures from pure ellipses.

Our two-dimensional galaxy model — built from the assorted one-dimensional profiles using the new *Cmodel* task (Ciambur 2015) within IRAF — has been subtracted from the original image to highlight the residual structure (Figure 3). This better reveals the elongated, off-center star cluster $\sim 5''$ (~ 400 pc) to the southeast of the galaxy center. We have subsequently discovered that this previously overlooked structure is also visible in the

² <https://hla.stsci.edu/>

³ <http://ast.noao.edu/data/software>

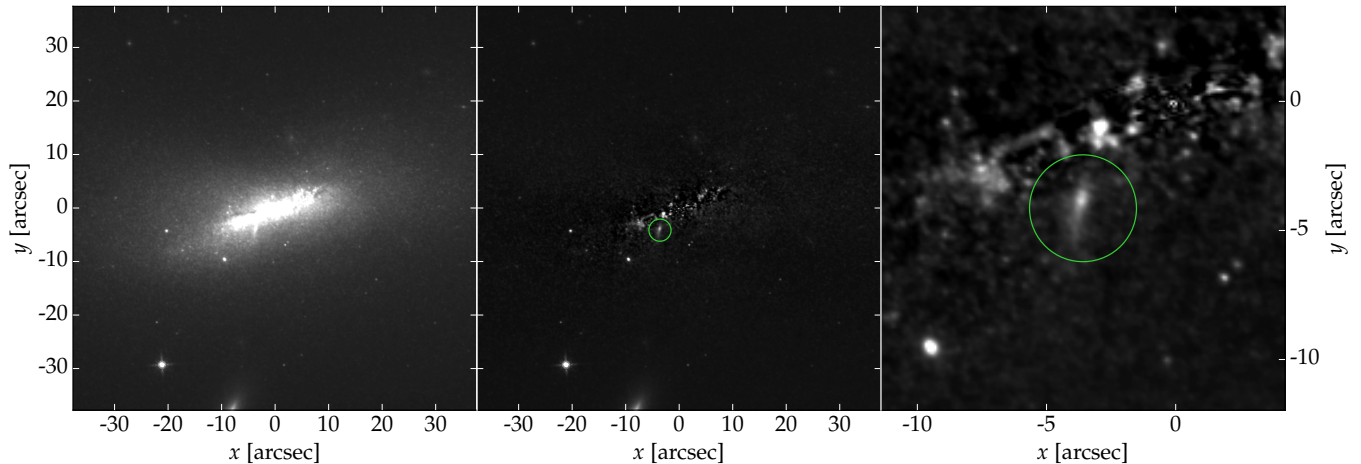


Figure 3. NGC 4424: *HST*/WFC3-IR F160W cut-out image (left panel: $88'' \times 88'' \approx 7\text{kpc} \times 7\text{kpc}$); *Isofit* residual image (middle panel); zoom-in of the region containing NGC 4424 X-3 (right panel).

F160W/F814W/F555W composite image made by Lisa Frattare, which can be seen at NASA’s website⁴ and in Graur et al. (2016, their Figure 1). Moreover, this star cluster is also where the off-centered X-ray point source resides (Figure 1, see also Boselli et al. 2018). This find, or realization, is reminiscent of the discovery of the optical counterpart/host of HLX-1 in the galaxy ESO 243-49 (Soria et al. 2010), which can be clearly seen in Figure 7 of (Ciambur 2015).

NGC 4424 contains a well-known, large-scale exponential-disk (Kenney et al. 1996; Cortés et al. 2006). Within this disk is a long faint-bar whose inner half has experienced a brightening, associated the boxy X/P structure or pseudobulge. The negative B_4 term at ~ 12 arcseconds (Figure 4) reflects the boxy isophotes of the bar/pseudobulge structure, as does the positive B_6 term. Given the unrelaxed nature of the system, this bulge may still be growing. At small radii ($R_{\text{eq}} < 3''$), knots along the major-axis give a disturbed appearance to the isophotes. Some of this has been captured by the model, evident by the spikes in the fourth- and sixth-order Fourier harmonic profiles (Figure 4). while most has been left behind in the residual image. The light profile in Figure 4 also displays a prominent upturn within the inner arcsecond. This may not originate from a single nuclear star cluster, but seems to reflect the unrelaxed state of play at the center of the galaxy where a few knots are seen.

The somewhat stretched star cluster in NGC 4424, which we shall refer to as ‘Nikhuli’ (see section 3.2), is drawn out in the direction of the galaxy’s center.

From the WFC3/IR F160W residual image (galaxy minus model), we measure this elongated source to have a flux of 879 ± 30 electrons per second. Using a WFC3/IR F160W zero-point⁵ of 25.946 mag (AB photometric system: Koekemoer et al. 2013), this corresponds to an apparent magnitude of 18.59 ± 0.04 mag (AB). Using a distance modulus of 31.08 ± 0.29 gives an absolute magnitude of -12.49 ± 0.29 mag. With an F160W absolute magnitude for the Sun of $+4.60$ mag (AB mag: Willmer 2018), the stellar luminosity is $(6.88 \pm 1.85) \times 10^6 L_{\odot, \text{F160W}}$. Assuming an F160W stellar mass-to-light ratio of 0.5 (Graham & Spitler 2009, see their Figure A1), the stellar mass is $(3.44 \pm 0.93) \times 10^6 M_{\odot}$. The Galactic extinction at $1.6 \mu\text{m}$, in the direction of NGC 4424, is just 0.01 mag (Schlafly & Finkbeiner 2011). From the 3-band composite color image in Graur et al. (2016), it also appears that dust intrinsic to NGC 4424 is not a significant issue at the location of Nikhuli.

2.2.1. Color

Given that Nikhuli is also visible in an F814W image, it rules out the possibility that the detection in the F160W image was solely due to Fe II $1.64 \mu\text{m}$ line emission from an ionized bubble around NGC 4424 X-3. The elongated morphology also disfavours such an interpretation. We used Gaussian smoothing to degrade the spatial resolution of the WFC3 UVIS channel F814W image—obtained from the same *HST* Proposal (ID 12880. PI: A.Riess) as the F160W image—to

⁴ <https://www.nasa.gov/image-feature/goddard/2017/hubbles-double-galaxy-gaze-leda-and-ngc-4424>

⁵ The sensitivity of the WFC3/IR detector has been remarkably stable over the past decade (Kozhurina-Platais & Baggett 2020) and offers a 1σ photometric accuracy/repeatability of 1.5% (0.015 mag) (Bajaj 2019).

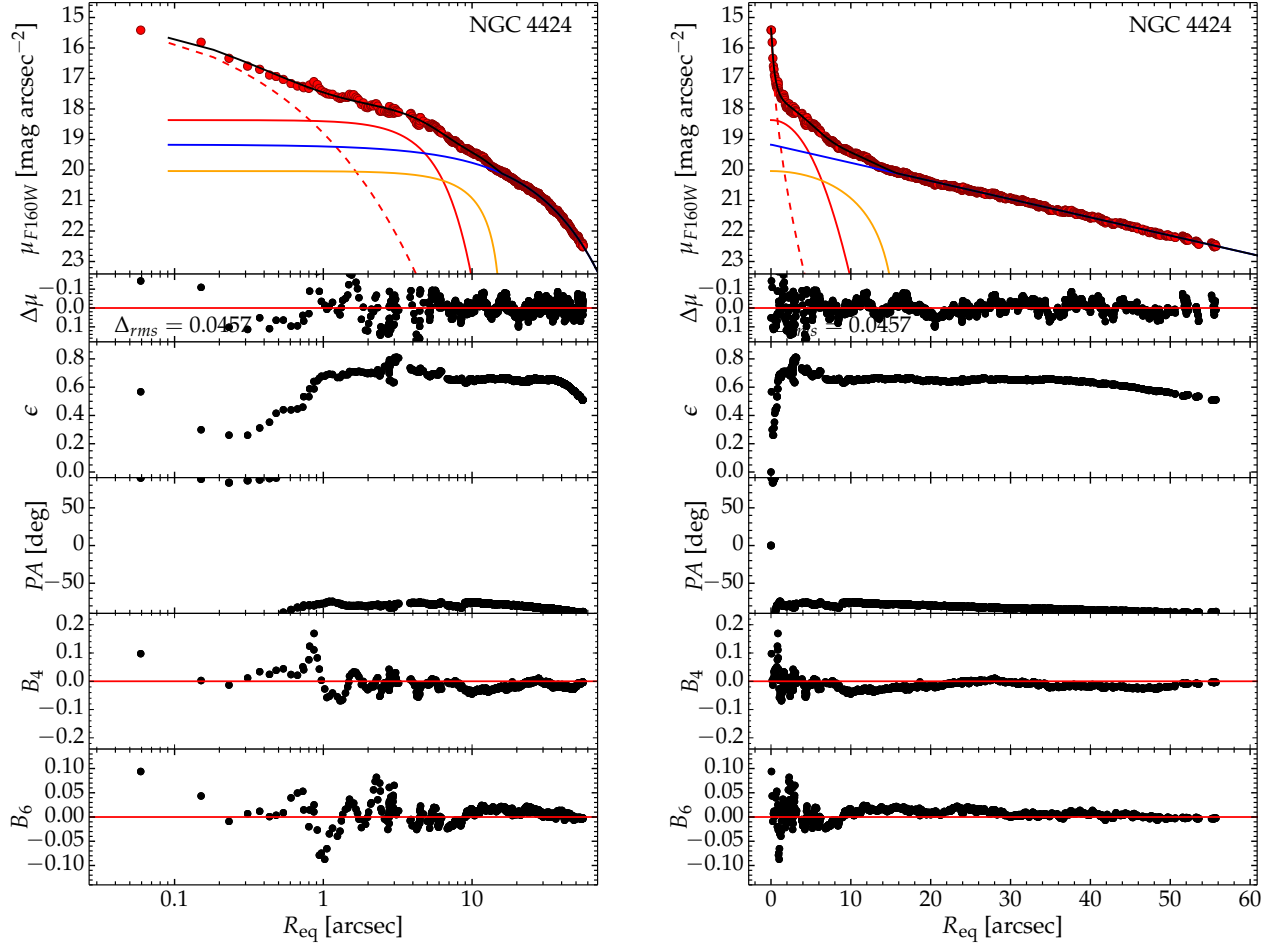


Figure 4. Geometric-mean axis, aka equivalent axis, of the *HST*/WFC3-IR F160W (*H*-band) light profile of NGC 4424. The galaxy light (red points) has been decomposed into structures using the PROFILER software (Ciambur 2016). While there is clearly a large-scale disk (dark blue), the unrelaxed nature of this post-merger remnant makes the inner components somewhat speculative. We have used a Ferrer bar component (orange), a Sérsic pseudobulge component (solid red), plus a Gaussian for the central star clusters (dashed red).

match the seeing in the F160W image. The (galaxy plus star cluster) light in a $3''.4$ (272 pc) by $1''.5$ (120 pc) ellipse centered on the star cluster has a mean F814W–F160W color equal to 1.60 ± 0.10 mag. This color is slightly redder than the surrounding mean galaxy color of 1.44 ± 0.04 mag, and may be indicative of an older stellar population. This would not be unusual. For example, the star cluster in the Milky Way dwarf spheroidal satellite Eridanus II is also thought to be old (Alzate et al. 2021).

Because the (color of the) galaxy light can dominate over the (color of the) star cluster light, the F814W–F160W galaxy (plus star cluster) color image is not optimal for showing the color of Nikhuli. We have, therefore, attempted to provide a color residual image rather than a color galaxy image. To do this, we subtracted the F160W residual image from the F814W residual image. By design, most of the pixels will have intensities close to zero in these residual images. As

such, the average ‘color’ in the color residual image will be close to zero rather than equal to the galaxy color. Furthermore, roughly half of the pixels in the F814W and F160W residual images have a negative intensity, especially where there was obscuration from dust. This can be problematic because the traditional color, given by the ratio of intensities, $-2.5 \log(I_1/I_2)$, is ill-defined when I_1/I_2 is negative, and the color image will be noisy where either I_1 or I_2 are close to zero. To mitigate against this, in the residual images we added a pixel intensity of 1 to those pixels with a positive intensity, and we subtracted a pixel intensity of 1 to those pixels with a negative intensity. For each of these modified residual images, we then calculated the pseudo-magnitudes $-2.5 \log(I + 1)$ for those pixels with positive values of I , and $+2.5 \log(|I - 1|)$ for those pixels with negative values of I . We then used $\text{mag}_1 - \text{mag}_2$ as our proxy for each pixel’s color. Due to the processes of image

rotation, alignment, pixel-size matching, seeing matching, plus our addition of the ‘bias level’ to the intensity, our pseudo-color image for the residual structure is not perfect, but it is still informative.

The prominent stripe seen in the pseudo-color residual image (Figure 5) is from the $1''.24$ -wide WFC3 UVIS detector chip gap in the F814W image. The yellow, three-pronged, fan pattern is due to Isofit more successfully capturing and removing this real galaxy structure from the F160W image than from the F814W image. While much of the blue color within the fitted quasi-elliptical region is noise, arising from zero minus zero, the image does reveal the relative intensity of F160W to F814W light in several features across the field. One can see that the light from Nikhuli (associated with emission in Figure 3) has a relatively high F160W to F814W intensity ratio. One can also see that the dust lane, associated with obscuration in Figure 3, and a studied feature in some spiral galaxy bars (e.g., Athanassoula 1992), also appears red. In contrast, an inner $3''.2$ (~ 260 pc) region of the disk, immediately east of the galaxy center, appears to have a relatively low F160W to F814W intensity ratio. This is indicative of recent/ongoing star formation. Unfortunately, the colors seen in Figure 5 are not perfect. A hindrance to a more quantitatively useful color residual image is the apparent lack of structure in the F814W image relative to the F160W image, which tends to amplify the signal from features in the F160W image. In addition, a galaxy model was independently fit to both the F160W and F814W images, and thus slightly different models have been subtracted from each image, affecting the build of the color image.

2.3. X-Ray data

2.3.1. Chandra X-Ray Observatory Data

Using the 14.87 ks *CXO* Advanced CCD Imaging Spectrometer (ACIS) exposure (ObsID: 19408. PI: Soria) taken on 2017-04-17, Boselli et al. (2018, see their sections 4.2) reported on the obscured X-ray source NGC 4424 X-3, located $4''.9$ (≈ 390 pc) to the southeast of the nucleus. The *CXO* enables accurate subarcsecond localizations of faint point-like sources and NGC 4424 X-3 is coincident with the star cluster.⁶ Figure 6 shows the X-ray point-source at R.A.=12:27:11.801, decl.=+9:25:10.71, with a red circle denoting the 90% radius = $0''.3$.

We have reanalyzed the *CXO* data following the detailed prescription provided in Graham et al. (2021) and Soria et al. (2021). Briefly, we used the Chandra Interactive Analysis of Observations (CIAO) Version 4.12 software package (Fruscione et al. 2006) with the Calibration Database Version 4.9.1, to reprocess the event files (CIAO task *chandra_repro*), and the display package DS9 (Joye & Mandel 2003) for image processing, centroiding, and selection of source and background regions. NGC 4424 X-3 is located close to the ACIS aim-point, which makes the point spread function sharper and reduces the positional uncertainty of the centroid even with a small number of counts. To take advantage of this, we also extracted images at sub-pixel resolution (0.5 pixels, corresponding to $\approx 0''.25$), with *dmcopy*, and used the 0.3–7 keV sub-pixel image for centroiding.

We used a source extraction radius of $1''.5$ (3 pixels) around the source centroid; the expected encircled energy within this radius is $\approx 95\%$. For the background, we used the annulus between $2''.5$ and $10''$. There are 8 X-ray counts within the source region (in fact, all within $1''.0$ of the centroid position), in the 0.3–7 keV band: none are in the soft band (0.3–1 keV), 1 is in the medium band (1–2 keV), and 7 are in the hard band (2–7 keV). Splitting the energy band in a different way, we see that all 8 counts are >1.5 keV. Although the number of counts is small, the detection is highly significant, because the background is very low; based on the local average, we expect only ≈ 0.1 background counts in the soft band, in the source region; ≈ 0.2 background counts in the medium band; and ≈ 0.1 background counts in the hard band. For $N = 8$ detected counts and ≈ 0.4 expected background counts in an integration time of 14.87 ks, the 90% Bayesian confidence interval is ≈ 4 –13 net counts, and the 99% interval is ≈ 2 –17 net counts (Kraft et al. 1991). The net 0.3–7 keV count rate (including the PSF correction to an infinite radius) is $0.56^{+0.42}_{-0.29} \times 10^{-3}$ ct s $^{-1}$ (90% Bayesian confidence interval).

We tried to infer more information on the flux and luminosity of X-3 in two different ways: from the energy of the detected photons (using the CIAO task *srcflux*) and by fitting a spectral model (using the XSPEC (Arnaud 1996) package version 12.11.0). First, we applied the *srcflux* task to the reprocessed event file to obtain a model-independent estimate of the observed,

⁶ The *CXO/HST* alignment was refined with the help of the point-like *CXO* source associated with the nucleus of the background galaxy at R.A.=12:27:12.16, decl.=+9:24:35.55 and with a quasar at R.A.=12:27:12.85, decl.=+9:24:13.13.

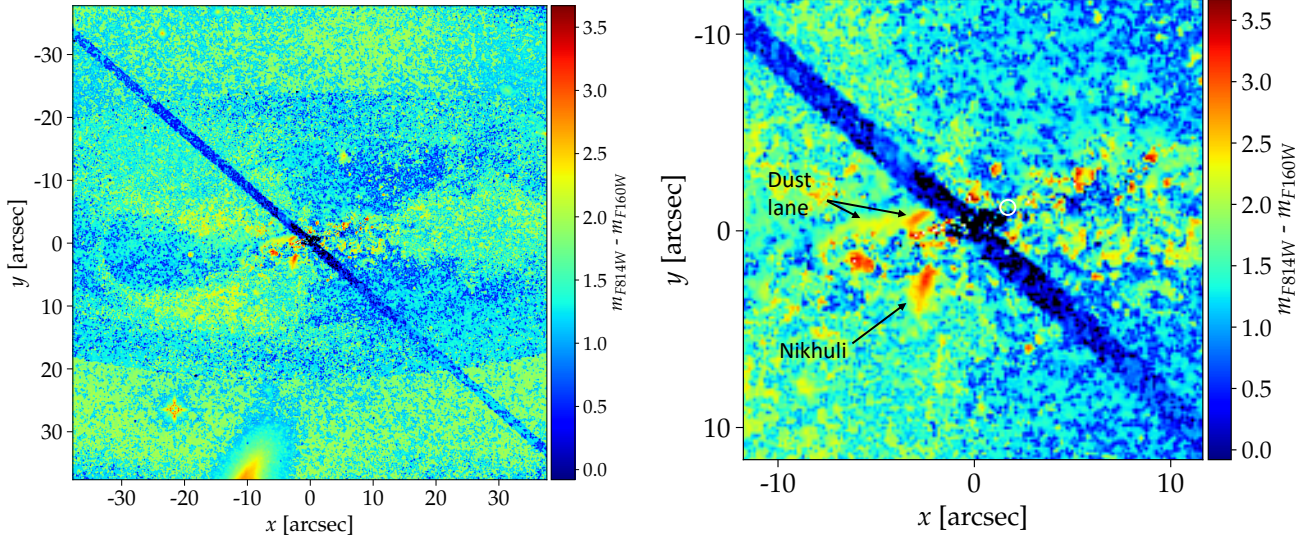


Figure 5. Pseudo-color residual image, and central zoom (right), after removing much of the mirror-symmetric component of NGC 4424 about its major axis. The WFC3-IR/F160W residual image (Figure 3) has been subtracted from the WFC3-UVIS/F814W residual image. The WFC3-UVIS chip gap is evident by the diagonal blue stripe. The galaxy center has been circled in white. Residual flux shows up as red or blue depending on whether the relative intensity in the F160W to F814W residual image is high or low. See section 2.2 for details.

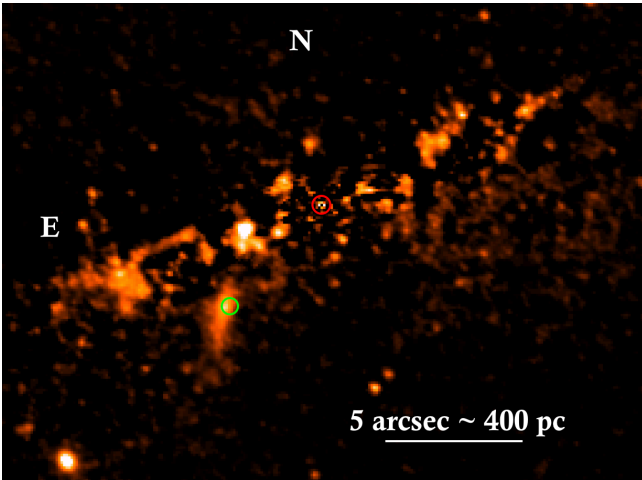


Figure 6. Residual image from Figure 3, with a slightly different contrast and with the center of the X-ray point-source NGC 4424 X-3 shown by the green circle. It has a radius of $0.''3$ and encapsulates the 90% uncertainty on the X-ray source position after mapping into the *HST* image. The red circle marks the center of the galaxy NGC 4424.

(HI gas)-dimmed, flux⁷ in the ‘broad’ ACIS band (0.5–7 keV). Second, despite the small number of counts, we extracted a spectrum and its associated response and ancillary response files with *specextract* (Figure 7). We regrouped the spectrum to 1 count per bin, and fitted it with simple models (power-law and disk-blackbody) using XSPEC. We used the (Cash 1979) statistics for the fit (*cstat* in XSPEC).

The main purpose of our spectral analysis was obviously not to determine a complex fitting model, but at least to estimate what intrinsic column density and de-absorbed luminosity are consistent with the peculiar energy distribution of the few observed photons (all above 1.5 keV). Assuming a power-law model (the simplest option in the absence of further information) with a photon index $\Gamma = 1.7$ (a standard, reference choice for the hard emission of accreting compact objects, e.g. Molina et al. 2009; Corral et al. 2011; Younes et al. 2011; Plotkin et al. 2013; Yang et al. 2015), we estimate that an intrinsic absorbing column $N_{\text{H,int}} \gtrsim 10^{22} \text{ cm}^{-2}$ (much higher than the Galactic line-of-sight col-

⁷ *srcflux*’s model-independent flux is based on the directly measured rate and energies of the detected photons, taking into account the quantum efficiency and effective area within the source region. Instead, the model-dependent flux is the flux of the best-fitting model to the observed photon distribution. They are alternative approximations to the ‘true’ observable (absorbed) flux. We used *srcflux* to calculate the model-independent flux, and XSPEC to determine the model-dependent flux. From XSPEC’s model-dependent flux we then computed the unabsorbed flux, and hence estimated the emitted luminosity.

umn density $N_{\text{H,Gal}} = 1.5 \times 10^{20} \text{ cm}^{-2}$; (HI4PI Collaboration et al. 2016)) is needed to explain the energy distribution of the detected photons (Table 1); a similarly high absorption is required if the spectral model is a disk-blackbody with an assumed temperature of 1.0 keV. This rough estimate of the intrinsic absorption permits a more realistic conversion of count rate and flux to intrinsic luminosity. For the assumed⁸ $\Gamma = 1.7$ power-law model⁹, the unabsorbed 0.3–10 keV luminosity is $L_{0.3-10} \approx 10_{-6}^{+14} \times 10^{38} \text{ erg s}^{-1}$. For the disk-blackbody model, $L_{0.5-8} \approx 9_{-5}^{+14} \times 10^{38} \text{ erg s}^{-1}$ (Table 1). As a further check of these results, we input the net count rates in the hard band (derived earlier with *srcflux*) into the CIAO version of the Portable, Interactive Multi-Mission Simulator (PIMMS) version 4.11a¹⁰, with response functions for Chandra Cycle 18. We recovered the same estimates for the intrinsic flux (corresponding to an extrapolated 0.3–10 keV luminosity of about $10^{39} \text{ erg s}^{-1}$ for plausible spectral slopes), and the same high values of $N_{\text{H,int}} \gtrsim 10^{22} \text{ cm}^{-2}$ to remove all photons below ≈ 1.5 keV. The *CXO* image is shown in Figure 1.

We do not have enough counts and bandwidth coverage to decide between a power-law model and a curved (e.g., disk-blackbody) model, even with the Cash statistics. A power-law model is the expected spectral shape for an IMBH, which would be in the low/hard state at a luminosity of $\approx 10^{39} \text{ erg s}^{-1}$ ($\sim 10^{-3}$ times the Eddington luminosity for a $10^4 M_{\odot}$ black hole). However, the luminosity of $\approx 10^{39} \text{ erg s}^{-1}$ is also consistent with a stellar-mass black hole at the top of the high/soft state, with a typical temperature of ≈ 1 keV and an inner disk radius ~ 50 – 100 km.

2.3.2. XMM-Newton data

The field around NGC 4424 X-3 was also observed with the *XMM-Newton* European Photon Imaging Camera - Metal Oxide Semi-conductor (EPIC-MOS) on two occasions: on 2010 June 13 (Obs.ID: 0651790101; Revolution: 1925) and 2017 December 5 (Obs.ID: 0802580201; Revolution: 3295), see Boselli et al. (2018, their Figure 5). We downloaded the data from the HEASARC archive and reprocessed them with the Sci-

Table 1. Best-fitting parameters of the Chandra/ACIS spectrum of NGC 4424 X-3.

Model Parameters	Values
Model-independent 0.5–7 keV flux from <i>srcflux</i>	
Net Rate ($10^{-3} \text{ ct s}^{-1}$)	$0.56_{-0.29}^{+0.42}$
$f_{0.5-7}$ ($10^{-14} \text{ erg cm}^{-2} \text{ s}^{-1}$)	$0.79_{-0.40}^{+0.59}$
<i>phabs</i> \times <i>phabs</i> \times <i>power-law</i>	
$N_{\text{H,Gal}}$ (10^{22} cm^{-2})	[0.015]
$N_{\text{H,int}}$ (10^{22} cm^{-2})	$2.7_{-1.9}^{+3.8}$
Γ	[1.7]
N_{po} ($10^{-6} \text{ photons keV}^{-1} \text{ cm}^{-2} \text{ s}^{-1}$ at 1 keV)	$4.5_{-2.8}^{+6.1}$
C-stat/dof	2.9/7
$f_{0.5-7}$ ($10^{-14} \text{ erg cm}^{-2} \text{ s}^{-1}$) ^a	$1.1_{-0.6}^{+1.0}$
$L_{0.3-10}$ ($10^{38} \text{ erg s}^{-1}$) ^b	$10.0_{-6.1}^{+13.7}$
<i>phabs</i> \times <i>phabs</i> \times <i>diskbb</i>	
$N_{\text{H,Gal}}$ (10^{22} cm^{-2})	[0.015]
$N_{\text{H,int}}$ (10^{22} cm^{-2})	$3.4_{-2.3}^{+4.6}$
kT_{in} (keV)	[1.0]
N_{dbb} (10^{-3} km^2) ^c	$1.3_{-0.8}^{+2.1}$
$R_{\text{in}} \sqrt{\cos \theta}$ (km) ^d	70_{-28}^{+43}
C-stat/dof	3.4/9
$f_{0.5-7}$ ($10^{-14} \text{ erg cm}^{-2} \text{ s}^{-1}$) ^a	$0.81_{-0.42}^{+0.69}$
$L_{0.3-10}$ ($10^{38} \text{ erg s}^{-1}$) ^b	$8.5_{-5.4}^{+13.5}$

Notes. Error ranges are 90% confidence limits for 1 interesting parameter. Values in brackets were frozen in the fit.

^a absorbed model flux in the 0.5–7 keV band.

^b isotropic de-absorbed luminosity in the 0.3–10 keV band, defined as $4\pi d^2$ times the de-absorbed 0.3–10 keV model flux.

^c $N_{\text{dbb}} = (r_{\text{in}}/d_{10})^2 \cos \theta$, where r_{in} is the apparent inner disk radius in km, d_{10} the distance to the source in units of 10 kpc (here, $d_{10} = 1640$), and θ is our viewing angle ($\theta = 0$ is face-on).

^d $R_{\text{in}} \approx 1.19 r_{\text{in}}$ for a standard disk (Kubota et al. 1998).

⁸ The power-law slope, aka photon index, Γ , is around 1.7 for Eddington ratios $\approx 10^{-5}$ – 10^{-2} (e.g. Molina et al. 2009; Corral et al. 2011; Younes et al. 2011; Plotkin et al. 2013; Yang et al. 2015). For Eddington ratios less than 10^{-5} , Γ steepens to around 2.1, and for Eddington ratios greater than 10^{-2} , Γ steepens to around 2.5.

⁹ With $\Gamma = 1.7$, one has that $L_{0.5-8 \text{ keV}} = 1.075 L_{0.5-7 \text{ keV}}$, and $L_{0.5-10 \text{ keV}} = 1.207 L_{0.5-7 \text{ keV}}$. Similarly, $L_{2-10 \text{ keV}} = 0.725 L_{0.5-8 \text{ keV}}$, and $L_{0.5-10 \text{ keV}} = 1.123 L_{0.5-8 \text{ keV}}$.

¹⁰ <https://cxc.harvard.edu/toolkit/pimms.jsp>

ence Analysis Software (SAS) (version 17.0.0: Gabriel et al. 2004). We rebuilt event files for the pn and MOS cameras with *epproc* and *emproc*, respectively. We filtered the event files to remove intervals of high or rapidly flaring particle background; we selected only intervals with a background RATE parameter < 0.35 for MOS1

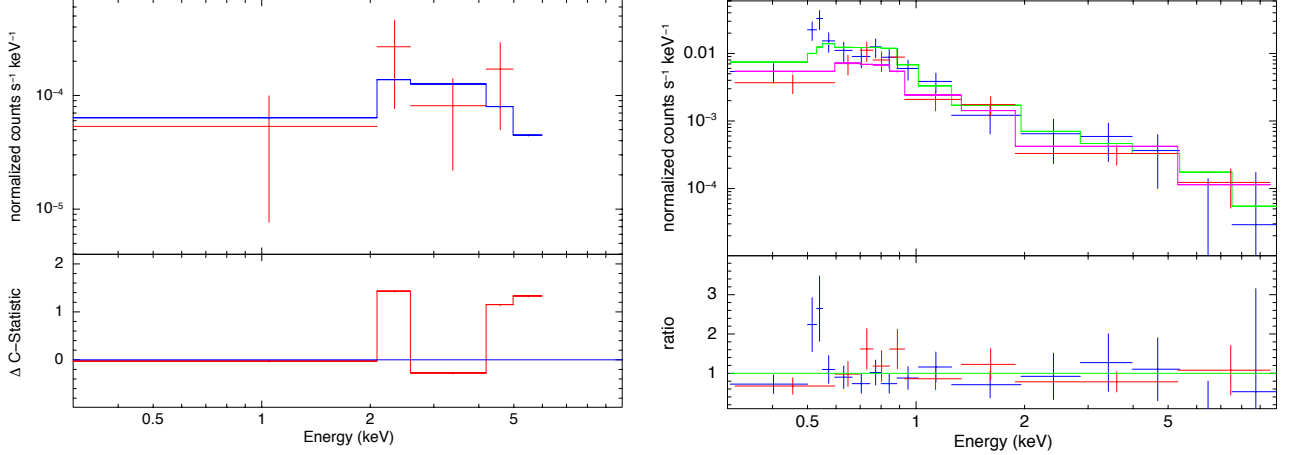


Figure 7. Left panel: CXO/ACIS-S spectrum of NGC 4424 X-3 in Nikhuli, with a $\Gamma = 1.7$ power-law model (blue line). The data points have been grouped to a signal-to-noise >1.8 for plotting purposes only. The fit was done on the individual counts, using Cash statistics. Right panel: Combined XMM-Newton/EPIC spectra of NGC 4424 X-3 in 2010 and 2017, along with the best-fitting models and the data/model ratios. Red data points are for the 2010 spectrum; the corresponding best-fitting model is plotted in magenta. Blue data points are for the 2017 spectrum; the corresponding best-fitting model is plotted in green. The EPIC spectra were grouped to 1 point per bin and fitted with the Cash statistics; the results were later rebinned to a signal-to-noise ratio >2.5 and a maximum number of grouped channels = 50, for plotting purposes only. The photon index (locked between the two epochs) of the power-law component is $\Gamma = 1.7^{+0.9}_{-0.7}$; the de-absorbed 0.3–10 keV luminosity of the power-law (i.e., not including the thermal plasma emission) is $\approx 10^{39}$ erg s⁻¹ in the 2010 EPIC spectrum and $\approx 2.2 \times 10^{39}$ erg s⁻¹ in the 2017 spectrum.

and MOS2, and <0.5 for the pn, at channels $10000 < \text{PI} < 12000$. After this filtering step, the good-time-interval for Obs.ID 0651790101 in the source extraction region was 13.8 ks for the pn, and 20.6 ks for each of the two MOS cameras; for Obs.ID 0802580201, the live time was 11.1 ks for the pn and 18.9 ks for the MOSs. We then filtered the event files with the standard conditions “(FLAG==0) && (PATTERN<=4)” for the pn, and “(#XMMEA_EM && (PATTERN<=12))” for the MOSs (corresponding to single and double events).

We defined a circular source region of radius $15''$: this is slightly smaller than usual for EPIC point-like sources, but we wanted to reduce contamination of the faint point-like source from the surrounding diffuse emission expected from the hot gas in the central region of this star-forming galaxy. (This is obviously not an issue in Chandra, given its much higher spatial resolution). We defined local background regions seven times larger than the source region. For each of the two observations, we used *xmmselect* to extract individual spectra for the pn and the MOSs; we built the associated response and ancillary response files with *rmfgen* and *arfgen*. Finally, we combined the pn and MOS spectra of each observation with *epicspeccombine*. We grouped the two resulting EPIC spectra to a minimum of 1 count per bin, and fitted them with XSPEC (Arnaud 1996) version 12.11.0, using the Cash statistics (Cash 1979). We chose the Cash statistics because the combined spectra

do not have enough counts for a meaningful χ^2 fitting: we estimate ≈ 190 net counts in the EPIC spectrum from Obs.ID 0651790101, and ≈ 120 net counts from Obs.ID 0802580201.

Both spectra are well fitted with thermal plasma emission, dominating below ≈ 1 keV, and a power-law component, dominating at higher energies. In particular, the soft component is consistent with multi-temperature thermal plasma. When fitted with a two *apec* components, the two temperatures are ≈ 0.2 keV and ≈ 0.7 keV. This is the characteristic temperature distribution of diffuse hot gas in star-forming galaxies (Owen & Warwick 2009; Mineo et al. 2012). Thus, we interpret the power-law component as the emission from the accreting compact object, and the soft component as a local enhancement of diffuse emission, tracer of recent star formation (perhaps associated with the satellite merger). The soft thermal component must be seen through a much lower column density than estimated from the hard colors of the Chandra detection.

Based on this tentative interpretation, and in order to limit the number of free parameters, we froze the temperatures of the two *apec* components at 0.2 keV and 0.7 keV, and added an additional intrinsic absorbing column density of 10^{22} cm⁻², seen only by the power-law component. We also kept the *mekal* normalizations and the power-law photon index locked between the two epochs. We obtain a good fit (C-statistics of 496.8/497) for a

photon index $\Gamma = 1.7^{+0.9}_{-0.7}$. The 0.3–10 keV deabsorbed luminosity of the power-law component (which corresponds to the point-like Chandra source, in our model interpretation) roughly doubled from $\approx 10^{39}$ erg s $^{-1}$ in 2010 to $\approx 2.2 \times 10^{39}$ erg s $^{-1}$ in 2017 (0.5–8 keV luminosities of $\approx 8 \times 10^{38}$ erg s $^{-1}$ and $\approx 1.8 \times 10^{39}$ erg s $^{-1}$, respectively).

In passing we note that because the X-ray source has not faded over 7 years, it is unlikely to have originated from a stellar tidal disruption event (TDE) from one of the stars in the star cluster approaching too close to the putative black hole (Baumgardt et al. 2006; Komossa 2015; Lin et al. 2018).

3. BLACK HOLE MASS ESTIMATES

NGC 4424 might harbour two massive black holes, possibly with one yet to settle to the center of this merged system (Merritt & Milosavljević 2005; Barausse 2012; Tremmel et al. 2018), thereby explaining NGC 4424 X-3 in the elongated, off-center star cluster. In this scenario, the second (speculated) massive black hole is quiescent, residing at the center of NGC 4424.

In what follows, we first report on the predicted mass for such a galaxy-centric black hole. We then provide a prediction for the mass of the black hole in the star cluster Nikhuli.

3.1. NGC 4424

Using a revised distance modulus of 31.080 ± 0.292 ($= 16.4 \pm 0.8$ Mpc), rather than 30.6 ± 1.0 , NGC 4424 has a revised (total) stellar mass $\log M_{*,\text{gal}} = 10.0 \pm 0.1$ (Graham et al. 2019, see their Appendix). This mass is based on the near-IR K' -band ($2.2 \mu\text{m}$) galaxy magnitude of 8.86 mag from GOLD Mine¹¹ (Gavazzi et al. 2003), plus our assumed 0.10 mag uncertainty and a K' -band stellar mass-to-light ratio for the galaxy of $M/L_{K'} = 0.62 \pm 0.09$. This galaxy stellar mass implies a central black hole mass of $\log M_{\text{bh}} = 4.8 \pm 0.8$ (based upon a symmetrical Bayesian analysis of the $M_{\text{bh}}-M_{*,\text{gal}}$ relation for late-type galaxies) or 5.1 ± 0.8 (based upon a symmetrical bisector regression for late-type galaxies using the modified FITEXY routine). See Davis et al. (2018) and Graham et al. (2019) for details.

The merger event in NGC 4424 may have elevated the central stellar velocity dispersion, reported to be 57.0 ± 8.6 km s $^{-1}$ by Ho et al. (2009). Although, this is perhaps in line with the (merger-induced increase to the) stellar mass as it results in a consistent prediction for the black hole mass of $\log M_{\text{bh}} = 5.0 \pm 0.8$ (Davis et al. 2017). The past/ongoing merger has, however, distorted the spiral

Table 2. Black hole mass predictions for the center of NGC 4424.

$\log M_{\text{bh}} (M_{*,\text{total}})$	$\log M_{\text{bh}} (\phi)$	$\log M_{\text{bh}} (\sigma)$	$\overline{\log M_{\text{bh}}}$
4.8 ± 0.8	6.7 ± 0.5	5.0 ± 0.8	4.9 ± 0.6

The predicted, central black hole masses shown here are in units of solar mass. As explained in Section 3, the predictions were derived from the galaxy’s total stellar mass, spiral arm pitch angle and stellar velocity dispersion. The pitch angle, however, is considered unreliable for predicting the black hole mass in this post-merger galaxy, and it is therefore not used to calculate the error-weighted mean black hole mass, $\overline{\log M_{\text{bh}}}$, shown in the final column. These masses should not be confused with the predicted, logarithmic black hole mass in Nikhuli, equal to 4.8 ± 1.6 (see the end of section 3).

pattern (Kenney et al. 1996; Cortés et al. 2006), likely accounting for the discrepant prediction, see Table 2, for the black hole mass obtained using the spiral arm pitch angle (16.9 ± 2.4 degrees: Graham et al. 2019) and the $M_{\text{bh}}-\phi$ relation in Davis et al. (2017).

The error-weighted mean of the logarithm of the estimated black hole masses can be calculated via

$$\overline{\log M_{\text{bh}}} = \frac{\sum_{i=1}^N w_i \log M_{\text{bh},i}}{\sum_{i=1}^N w_i}, \quad (1)$$

with inverse-variance weighting¹² such that $w_i = 1/(\delta \log M_{\text{bh},i})^2$. The associated 1σ standard error is given by

$$\delta \overline{\log M_{\text{bh}}} = \sqrt{1 / \sum_{i=1}^N w_i}. \quad (2)$$

Based on the stellar mass and velocity dispersion of NGC 4424, it is predicted to possess a central intermediate mass black hole with $\overline{\log M_{\text{bh}}} = 4.9 \pm 0.6$ dex. The benefit of such an error-weighted mean is that the uncertainty is less than the near-order of magnitude uncertainty on the individual black hole mass estimates.

3.2. Nikhuli

The elongated star cluster likely represents the nucleus of a captured galaxy undergoing the final digestion stages of merging and assimilation with NGC 4424. As the likely inner seed of a galaxy harvested from the nearby environment and consumed by NGC 4424, we

¹¹ <http://goldmine.mib.infn.it/>

¹² This gives the ‘maximum likelihood estimate’ for the mean of the probability distributions under the assumption that they are independent and normally distributed with the same mean.

refer to this star system as Nikhuli¹³, which is a name relating to a festive period of celebrating and wishing for a rich harvest.

The central black hole of Nikhuli, should one exist, might be smaller than the above prediction, and thus also of intermediate-mass (10^2 – $10^5 M_\odot$). [Graham \(2020\)](#) has found that the M_{bh} – M_{nsc} relation for nuclear star clusters (NSCs) also applies to ultracompact dwarf (UCD) galaxies, thought to be the tidally stripped nuclei of galaxies ([Zinnecker et al. 1988](#); [Freeman 1993](#); [Ferrarese et al. 2016](#)). Nikhuli likely represents such a system. From a visual inspection of the ‘residual image’ of NGC 4424, it is hard to establish how much of the infalling nuclear star cluster may have been stripped away, or instead, how much of the infalling galaxy still remains around the infalling nuclear star cluster. Nonetheless, we can employ equation 7 from [Graham \(2020\)](#), which relates the stellar mass of nuclear star clusters to their central black hole mass. The relation can be written as

$$\log(M_{\text{bh}}/M_\odot) = (2.62 \pm 0.42) \log(M_{\text{nc}}/[10^{7.83} M_\odot]) + (8.22 \pm 0.20), \quad (3)$$

with the uncertainty on the black hole mass given by the expression

$$(\delta \log M_{\text{bh}}/M_\odot)^2 = [\log(M_{\text{nc}}/[10^{7.83} M_\odot])]^2 (0.42)^2 + (0.20)^2 + (2.62)^2 [\delta \log M_{\text{nc}}]^2 + \epsilon^2.$$

The term $\delta \log M_{\text{nc}}$ is the uncertainty associated with the nuclear star cluster’s stellar mass, and ϵ is the intrinsic scatter in the $(\log M_{\text{bh}})$ -direction, and taken to be 1.31 dex ([Graham 2020](#)).

Assigning a factor of 2 uncertainty to the total stellar mass of the stretched star cluster, one obtains a (poorly constrained)¹⁴ value of $\log(M_{\text{bh}}/M_\odot) = 4.83 \pm 1.63$, corresponding to $M_{\text{bh}} = 7 \times 10^4 M_\odot$ when expressed in linear units. For reference, due to the steep (2.62) slope of the M_{bh} – M_{nsc} relation (Equation 3), a factor of 2 reduction to the star cluster mass results in a large 0.8 dex decrease to the predicted black hole mass in the star cluster. This black hole mass should not be confused with the above predictions for a *central* massive black hole in NGC 4424.

For the potential nuclear star cluster already at the center of NGC 4424, if it has been experiencing continuous star formation for the past 0.5 Gyr ([Boselli et al.](#)

2018), then the associated M/L_H ratio could be as low as 0.13, or half that value if the star formation started 0.1 Gyr ago ([Busch et al. 2014](#), see their Figure 13). This uncertainty, coupled with the dust extinction at the center of the galaxy, which is evidently not negligible in the H -band, makes it problematic to ascertain a reliable mass for the potential nuclear star cluster at the center of NGC 4424. We have, therefore, not attempted to estimate a stellar mass.

From $L_X \equiv L_{0.5-10 \text{ keV}} = 7.09 \times 10^{38} \text{ erg s}^{-1}$ (Table 1), the Eddington ratio (L_X/L_{Edd}) of NGC 4424 X-3 can be calculated using $L_{\text{Edd}} = 1.3 \times 10^{38} M_{\text{bh}}/M_\odot \text{ erg s}^{-1}$. Given the above black hole mass estimate of $7 \times 10^4 M_\odot$, the Eddington ratio is 8×10^{-5} , or roughly 10^{-4} . Such a value is typical of those seen in the few active IMBH candidates at the centers of early-type galaxies in the Virgo cluster ([Graham & Soria 2019](#), their Figure 8). Alternatively, NGC 4424 X-3 could be a 5.5 solar mass black hole radiating at the Eddington limit.

3.2.1. X-ray Binaries

The likelihood of NGC 4424 X-3 being a compact stellar mass object, and XRB, such as an accreting neutron star or a stellar-mass black hole, is not high.

High-mass X-ray binaries (HMXBs), in which the donor star has a high mass, obviously requires a young donor star. However, the morphology and red color of Nikhuli suggests that it consists of an older, evolved, stellar population, thereby disfavoring a HMXB in Nikhuli. We can estimate the probability of a field HMXB in NGC 4424 having a chance alignment with Nikhuli by using the knowledge that the abundance of HMXBs scales with the galaxy star-formation rate ([Sunyaev et al. 1978](#); [Ghosh & White 2001](#); [Grimm et al. 2003](#); [Fragos et al. 2013](#)). [Boselli et al. \(2015\)](#) report a global star formation rate of $0.32 M_\odot \text{ yr}^{-1}$ in NGC 4424, rescaled from 23 Mpc to our distance of 16.4 Mpc, while [Boselli et al. \(2018\)](#) revise this down further to $0.25 M_\odot \text{ yr}^{-1}$. This corresponds to a specific star-formation rate of $\log(\text{sSFR yr}^{-1}) \approx -10.4$, based on $M_{*,\text{gal}} = -9.8 \pm 0.4$ ([Graham et al. 2019](#)). For $\Gamma = 1.7$, the X-ray point-source in Nikhuli has $L_{0.5-8 \text{ keV}} \approx 6 \times 10^{38} \text{ erg s}^{-1}$. Now, from [Lehmer et al. \(2019\)](#), one therefore expects just two HMXBs with $L_{0.5-8 \text{ keV}} \geq 6 \times 10^{38} \text{ erg s}^{-1}$ across the galaxy’s ~ 9 square arcminutes of star-forming area, thereby making the arcsecond-alignment of NGC 4424 X-3, should it be a HMXB, with Nikhuli an extremely unlikely coincidence.

We can also explore the probability that NGC 4424 X-3 is a low-mass X-ray binary (LMXB). The X-ray luminosity function of LMXBs scales with the stellar mass. From [Lehmer et al. \(2019\)](#), one again expects

¹³ Taken from the Sumi language, spoken by a quarter of a million (formerly all tribal) people in Nagaland, the name relates to the Tuluni, *aka* Anni, festival. (Many Naga tribes are known to have been headhunters into the 19th and 20th century.)

¹⁴ The heightened uncertainty is due to the steep slope of, and scatter about, the M_{bh} – M_{nsc} relation.

around two LMXBs with $L_{0.5-8\text{ keV}} \geq 6 \times 10^{38} \text{ erg s}^{-1}$ per $10^{11} M_{\odot}$, or 0.7×10^{-4} per $3.44 \times 10^6 M_{\odot}$, which is the mass of Nikhuli. However, this expectation is based upon field star statistics. The number of LMXBs in globular clusters is $\sim 10^3$ times greater than in the field (Sivakoff et al. 2007; Kim et al. 2013; Lehmer et al. 2020). As a former nuclear star cluster, Nikhuli may thus have a $\sim 7\%$ chance of being an LMXB, *if* globular clusters and nuclear star clusters have a similar LMXB formation efficiency. This is the only realistic chance NGC 4424 X-3 has of being an XRB rather than a massive black hole. However, supermassive black holes and nuclear star clusters are known to regularly coexist in galaxies with $10^6 < M_{\text{bh}}/M_{\odot} < 10^7$ (e.g. Graham & Spitler 2009, and references therein), and thus the infall origin for Nikhuli *may* favor the presence of an active massive black hole rather than an XRB.

4. INFALL TIMESCALE

Lacking an outward-pointing, comet-like appearance, we suspect that this active¹⁵ star cluster is probably not an ejected nucleus from a gravitational wave recoil event (Blecha & Loeb 2008; Holley-Bockelmann et al. 2008; Komossa & Merritt 2008; Askar et al. 2021; Hogg et al. 2021; Ward et al. 2021). Although probably evident to many readers, we note that Nikhuli has a lopsided shape, unlike that of a (background) galaxy. The significant elongation of Nikhuli in the direction of the NGC 4424 galaxy center favors an infall scenario. Conceivably, three additional knots to the north may delineate the orbital path of the infalling galaxy. Tidal stretching (Roche 1850) of an accreted nuclear star cluster, and possibly the paltry remains of the accreted galaxy still surrounding the nuclear star cluster, is evident.

There is an abundance of nucleated dwarf and nucleated spiral galaxies (Böker et al. 2002; Graham & Guzmán 2003), and their nuclear star cluster can contain a massive black hole (e.g. Graham & Spitler 2009). The accretion of these galaxies, coupled with dynamical friction, can drive their nuclear star clusters toward the center of the accreting galaxy. Massive structures, such as dense star clusters, can sink due to the braking force and thus orbital decay, arising from the dynamical friction with the surrounding galaxy (Chandrasekhar & von Neumann 1943; Baranov & Batrakov 1974; Tremaine et al. 1975; Inoue 2011; Arca-Sedda & Capuzzo-Dolcetta 2014a,b; Chen et al. 2021; Morton et al. 2021).

Differing from the *naked*¹⁶ black holes in the merger simulations of Bellovary et al. (2021) and Ma et al. (2021), which tend not to sink to the center of the final galaxy but remain off-center, the *shrouded* black hole in Nikhuli may have more success (Pfister et al. 2019; Ma et al. 2021). Bekki (2010) have shown that star clusters with masses greater than $2 \times 10^5 M_{\odot}$, i.e., less than 10 times the mass of Nikhuli, experience significant orbital decay within 1 Gyr. Other simulations have found that black holes can form close pairs in dwarf galaxies, which likely merge to build the foundation of the central supermassive black hole and produce gravitational wave signals detectable using the planned Laser Interferometer Space Antenna (e.g., Bellovary et al. 2019). In addition, Oh & Lin (2000) report that globular cluster capture may explain some of the nucleated dwarf galaxies in the Virgo cluster, with the clusters reaching the core within a Hubble time.

Following Binney & Tremaine (1987, their eq. 7.18), a crude estimate for the time, t , it would take Nikhuli (with NGC 4424 X-3) to sink to the center of NGC 4424 can be made when assuming the inner region of NGC 4424 is dominated by stars with a roughly homogeneous, isothermal distribution. Their dynamical friction timescale is given by

$$t = \frac{264}{\ln \Lambda} \left(\frac{10^6 M_{\odot}}{M} \right) \left(\frac{r}{2 \text{ kpc}} \right)^2 \left(\frac{v_c}{250 \text{ km s}^{-1}} \right) \text{ Gyr.} \quad (4)$$

While Carollo (1999) adopted $\log \Lambda = 10$ for Coulomb's logarithm, we use $\ln \Lambda = 10$, which is 2.3 times smaller. Substituting in $M = 3.44 \times 10^6 M_{\odot}$ for Nikhuli, along with $r = 400 \text{ pc}$ and $v_c = \sqrt{2}\sigma$, where $\sigma = 57 \text{ km s}^{-1}$, one obtains a dynamical friction time of $\sim 100 \text{ Myr}$. If one assumes that Nikhuli is at a non-projected distance of 1 kpc from the galaxy center, then one obtains a timescale of $\sim 0.64 \text{ Gyr}$. Such timescales mesh well with those seen in Lotz et al. (2001, see their Figure 2), who used a value of $\ln \Lambda \approx 7.3$. If we adopt the value $\log \Lambda = 2$ found by Velazquez & White (1999) for bulgeless, exponential disks in dark matter halos with NFW (Navarro et al. 1996) profiles, then the above timescales increase to ~ 0.5 and $\sim 3.2 \text{ Gyr}$. However, as Milosavljević (2004) note, disk perturbations, which can include spiral arms and bars, can result in both positive and negative torques on an infalling satellite. The bar-like feature in NGC 4424 may facilitate the inspiral of the Nikhuli/black hole system (Bortolas et al. 2021). Whether or not Nikhuli makes it all the way to the cen-

¹⁵ We use the term ‘active’ to denote a star cluster with an active black hole; in this case, X-ray active.

¹⁶ The term ‘naked’ is used to denote the absence of a surrounding star cluster.

ter of NGC 4424, and how long that may take, will also depend on the time spent in the disk plane and requires modeling beyond the scope of this paper.

In low-mass spheroids with low Sérsic indices, and thus a shallow gradient to their central gravitational potential (e.g., Terzić & Graham 2005; Terzić & Sprague 2007), star clusters can wander about their galaxy’s center, typically displaced by ~ 100 parsecs (Binggeli et al. 2000). Massive black holes can also be offset (Boldrini et al. 2020; Ricarte et al. 2021). A similar situation occurs in the partially depleted cores of massive spheroids, where infalling perturbers can stall outside of the cores with shallow density profiles (Goerdt et al. 2006; Read et al. 2006; Inoue 2009; Petts et al. 2015; Bonfini & Graham 2016; Banik & van den Bosch 2021). However, Figure 3 does not suggest that Nikhuli has stalled, and as such we can not conclude that Nikhuli is destined to become an eternally wandering black hole. We can, however, derive an additional estimate of the dynamical friction time scale for a shallow potential.

Assuming that Nikhuli is now orbiting within the pseudobulge of NGC 4424, and assuming this pseudobulge dominates the inner gravitational potential, we can use the Sérsic function which was found to describe this structure (Figure 4) to estimate the infall time for Nikhuli. Building on Arca-Sedda & Capuzzo-Dolcetta (2014a, their equation 21), Arca-Sedda et al. (2015, their equation 8) provide an (orbital eccentricity)-dependent variant from which the following expression was obtained. The equation depends on the inner profile slope and yields the time an infalling star cluster of mass M_{sc} at radius r will take to get to the center of a bulge/halo with mass M_b , scale radius r_s , and negative logarithmic slope of the inner density profile γ_0 .

$$t(\text{Myr}) = 0.3 \sqrt{\frac{(r_s/\text{kpc})^3}{(M_b/10^{11} M_\odot)}} g(e, \gamma_0) \left(\frac{M_b}{M_{sc}}\right)^{0.67} \left(\frac{r}{r_s}\right)^{1.76} \quad (5)$$

From our fitted Sérsic function, we derived a mass for the pseudobulge¹⁷ such that $\log(M_b/M_\odot) = 8.48 \pm 0.34$, assuming $M/L_{F160W} = 0.5$. This is notably greater than the mass of Nikhuli with $M_{sc} = (3.44 \pm 0.93) \times 10^6 M_\odot$, which we take to be at a deprojected radius $r = 5''$ (395 pc) from the center of NGC 4424. Graham et al. (2006, their equation 23) provide an equation for the negative logarithmic slope, γ_0 , of the model from Prugniel & Simien (1997), which uses the Sérsic model

parameters to provide an expression which approximates the deprojected Sérsic (1963) $R^{1/n}$ model. For small radii, γ_0 depends solely on n . We found the pseudobulge in NGC 4424 is well-described with $n = 0.47 \pm 0.08$, for which we obtain $\gamma_0 \approx 0$. Arca-Sedda et al. (2015, their equation 5) provide an expression to derive the appropriate scale radius r_s from the projected ‘effective half-mass radius’ of the bulge/halo — taken here to be the ‘effective half-light radius’ of our equivalent-axis (*aka* geometric-mean axis) model for the pseudobulge. With $R_{e,eq} = 3''.87 \pm 0''.39$ from our Sérsic model fit to the pseudobulge, we have that $r_s \approx 0.35 R_{e,eq} = 1''.35$, or ≈ 106 pc. Finally, for an eccentricity $e = 0$ and $\gamma_0 = 0$, the $g(e, \gamma_0)$ term above, from Arca-Sedda et al. (2015, their equation 10), equals 5.83. Inserting the above values into equation 5, one obtains a dynamical friction time of 220 Myr.

Alternatively, we can approximate the total (bulge + bar + disk) light over ~ 1 to ~ 8 arcseconds in Figure 4 with an $n = 1$ model having a half-light radius of $8''.4$. The stellar mass of this model, within this half-light radius, is approximately $0.8 \times 10^9 M_\odot$, with an extrapolation of the profile to infinity doubling this mass to $1.6 \times 10^9 M_\odot$. Under the approximation of a spherical system, this model corresponds to $\gamma_0 = 0.44$, $r_s = 3''.5$ (277 pc), and $g(e, \gamma_0) \approx 5.2$, and it yields a similar infall time of 206 Myr. Increasing the assumed distance of Nikhuli from the galaxy center by a factor of 3 lengthens the infall time to ~ 1.4 Gyr, while assuming an eccentricity of 0.5 will reduce the times by a factor of 0.65, giving $t = 0.9$ Myr in this instance. The star cluster(s) seen within the inner arcsecond may be a testament to these dynamical times.

5. DISCUSSION

The phenomenon of an infalling galaxy undergoing assimilation has been offered to explain the offset IMBH in ESO 243-49 (Farrell et al. 2009; Bellovary et al. 2010; Mapelli et al. 2012; Webb et al. 2017; Bellovary et al. 2021; Ricarte et al. 2021) and the ULX sources likely associated with a massive black hole in galaxies such as IC 4320 (Sutton et al. 2012), NGC 5252 (Kim et al. 2015, 2020), NGC 2276-3c (Mezcua et al. 2015) and others. One such interesting example can be seen in the Virgo cluster galaxy NGC 4651 (Martínez-Delgado et al. 2010; Foster et al. 2014; Morales et al. 2018), where the elongation process associated with infall has produced a tidal stream (Newberg 2016) which is immediately evident in optical images. An earlier stage of such shredding, of an infalling dwarf galaxy, has been reported in a galaxy at a redshift $z = 0.145$ by Forbes et al. (2003). See also UGC 10214 (Vorontsov-Vel’Yaminov 1959; Miskol-

¹⁷ Using the pseudobulge mass in the $M_{bh}-M_{bulge}$ relation for late-type galaxies (Davis et al. 2019; Sahu et al. 2019) gives a predicted black hole mass of $\log(M_{bh}/M_\odot) = 3.8$. However, the unrelaxed nature of this pseudobulge makes this a dubious prediction.

ezi et al. 2011), NGC 7714 (Soria & Motch 2004), and M32 giving itself to M31 (Arp 1964; Graham 2002; Gordon et al. 2006). Various stages of the interaction process are evident in the catalog of Vorontsov-Velyaminov (1977), and the scenario in which a galaxy is threshed and reduced to its dense core has been developed by (Bekki & Freeman 2003).

In and around our Galaxy, we know that the Sagittarius dwarf galaxy is undergoing disruption (Ibata et al. 1994; Koposov et al. 2015), the Cetus and Indus stellar streams are the remnants of accreted dwarf galaxies (Chang et al. (2020); Hansen et al. (2021)), and the Gaia-Enceladus-Sausage was acquired long ago (Belokurov et al. 2018; Helmi et al. 2018). Furthermore, Ibata et al. (2019a) revealed the impressive tidal stream associated with ω Centauri, possibly the pared-core of an accreted dwarf galaxy but currently lacking confirmation of a central black hole (Zocchi et al. 2019; Baumgardt et al. 2019). Additional globular cluster streams, evidence of accretion and possibly remnant galaxy nuclei in the Milky Way are known (e.g. Bonaca et al. 2021; Woody & Schlafman 2021; Pfeffer et al. 2021; Thomas et al. 2020; Ferguson et al. 2021; Piatti et al. 2021). Yuan et al. (2020) and Malhan et al. (2021) discovered and investigated the low-mass stream LMS-1, revealing the remnants of a low-mass galaxy now just 10 to 20 kpc from our Galaxy’s center, making it the closest known stream to the Galaxy’s center thus far. They conclude that the “globular cluster” NGC 5024 or NGC 5053 is likely the former nuclear star cluster of this low-mass galaxy, akin to NGC 5824 possibly being the remnant nuclear star cluster of the dwarf progenitor to the Cetus stream (Chang et al. 2020). The slightly more massive (than globular cluster) UCD galaxies (e.g. Ahn et al. 2017) have also been caught in the act of stripping. They are considered to be the former nuclei of galaxies (e.g., VUCD3: Liu et al. 2015) and are known to contain massive black holes (Graham 2020, and references therein).

Globular clusters are known to contain XRBs (e.g. Hut et al. 1992; Becker et al. 2003; Maccarone et al. 2003), and it has been speculated that their capture may contribute to the LMXB population in galaxies (Lehmer et al. 2020). With a stellar mass of $\sim 3 \times 10^6 M_\odot$, Nikhuli is more massive than most globular clusters. Furthermore, the width of the Nikhuli stream is some 35 pc across. As such, we are probably not seeing a captured globular cluster—which have half light radii typically less than 4 pc (Jordán et al. 2005)—but more likely the nucleus of a stripped galaxy. Conceivably, the color or metallicity of Nikhuli might shed light on the full stellar mass of the progenitor via the color-magnitude or mass-

metallicity relation for dwarf galaxies. However, given that the remnant nuclear star cluster light will now dominate the flux and color, this would yield questionable results.

Although Nikhuli is unlikely to be a captured globular cluster, if nuclear star clusters have a similar LMXB formation efficiency as globular clusters, then Nikhuli might contain a LMXB. It would therefore be desirable to observe Doppler-broadened, optical emission lines coming from NGC 4424 X-3 to verify the existence of the potential massive black hole. Such confirmation of a massive black hole mass might be possible if (with sufficiently high spatial resolution in order to reduce the stellar noise) broad optical emission lines are observed from NGC 4424 X-3. An alternative approach to estimate the black hole mass could come from the ‘fundamental plane of black hole activity’. As given by Plotkin et al. (2012), it predicts a radio luminosity $\nu L_\nu(5 \text{ GHz})$ of $10^{33.9} \text{ erg s}^{-1}$ for $M_{\text{bh}} = 0.7 \times 10^5 M_\odot$ and $L_{0.5-10 \text{ keV}} = 0.7 \times 10^{39} \text{ erg s}^{-1}$. At a distance of 16.4 Mpc, this corresponds to 5 μJy , tantalizingly within the reach of the Karl G. Jansky Very Large Array (VLA) and the Australia Telescope Compact Array (ATCA), which have probed down to root mean square (rms) noise levels of $\sim 1-2 \mu\text{Jy beam}^{-1}$ (Strader et al. 2012; Tremou et al. 2018).

An incoming black hole of equal mass to that already (presumed to be) at the center of NGC 4424 might imply a major merger between two spiral galaxies. However, such a scenario is unlikely to result in a post-merger galaxy looking like a spiral galaxy. On the other hand, early-type galaxies have smaller stellar masses for a given black hole mass than late-type galaxies (Sahu et al. 2019). As such, a minor merger *can* bring in an equal mass black hole. This suggestion, which we think is presented here for the first time, may also explain why the extreme ULX and HLX off-center sources found by Sutton et al. (2012) in eight nearby (<100 Mpc) galaxies are not in galaxies displaying signs of a recent major merger.

A minor merger in NGC 4424 also meshes with the notion of an unequal (stellar mass) merger reported by Boselli et al. (2018). From Figure 11 in Sahu et al. (2019), one can see that an early-type galaxy with a black mass of $10^{4.8} M_\odot$ (see section 3.2) will have a stellar mass of $\sim 0.6 \times 10^9 M_\odot$, which is just 6% of the stellar mass of NGC 4424 (see section 2.2). Suppose such an early-type galaxy is what fell into NGC 4424. In that case, (ignoring gaseous processes), the coalescence of NGC 4424’s initial and incoming black hole will double the central black hole mass, with the stellar mass increasing by only $\sim 6\%$. We speculate that such minor mergers may help maintain the steepness of the non-

linear, near-cubic $M_{\text{bh}}-M_{*,\text{gal}}$ relation for spiral galaxies (Savorgnan et al. 2016; Davis et al. 2018). Furthermore, compact spheroids and the bulges of early-type galaxies formed early in the Universe (Graham et al. 2015, and references therein) and were likely the formation sites of the first massive black holes. Some of these galaxies (and their black holes) may have subsequently been sewn (and sown) into late-type spiral galaxies.

Given the similarity of the predicted (central and infalling) black hole masses in NGC 4424, and the absence of an X-ray point source at the (very) center of NGC 4424, it might, but need not, be the case that NGC 4424 currently has no central black hole. The delivery of NGC 4424 X-3 via a low-mass early-type galaxy might demonstrate how some apparently bulgeless late-type galaxies, like, for example, M33 (Merritt et al. 2001), could eventually be both seeded with massive black holes and commence building their bulge. The median bulge-to-total flux ratios in Sc and Sd galaxies are only 8% (Graham & Worley 2008). The bulge growth from minor mergers might be slow at first, and initially go undetected while the bulge-to-total stellar mass ratio is small or ill-defined, leading to ‘bulgeless galaxies’ with massive black holes, such as NGC 4395, NGC 2748 and NGC 6926 (Davis et al. 2019). Indeed, Cortés et al. (2006) has suggested that NGC 4424 will become a lenticular galaxy with a small bulge over the next 3 Gyr. The merger-induced bulge growth arises not just from the delivery of new stellar material sewn into the galaxy, but also from the redistribution of gas toward the galaxy center, which subsequently undergoes star formation.

In a downsizing scenario, such minor mergers would represent the late-time seeding of massive black holes into late-type spiral galaxies. Seeding by accretion may, of course, occur over a range of redshifts. This is different to high- z quasars getting a kick start in life from a ‘black hole seed’ that is an IMBH (e.g., Düchting 2004; Koushiappas et al. 2004), unless the origin of massive black holes in dwarf early-type galaxies is the same as high- z quasars. While the old nuclear star clusters of five low-mass dwarf early-type galaxies (Paudel et al. 2011) may support this, those clusters could represent globular clusters captured through dynamical friction. Furthermore, it is not yet clear that today’s dwarf early-type galaxies, a source of minor mergers for spiral galaxies, ubiquitously contain a massive black hole. Although Graham et al. (2021) report that the detection of an X-ray point-source at the center of low-mass late-type galaxies is $\sim 40\%$, while it is just $\sim 10\%$ in low-mass early-type galaxies, they suggest that this may reflect the availability of cold gas for igniting the candidate

AGN in these galaxies, rather than representing a measure of the massive black hole occupation fraction. Further work is required to establish the true massive black hole occupation fraction in low-mass galaxies.

In addition to a ‘classical’ (i.e., merger built) bulge, an incoming perturber might cause a thin in-plane bar to experience an instability leading to the creation of an X/(peanut shell)-shaped ‘pseudobulge’ structure (Combes et al. 1990; Athanassoula 2005; Ciambur & Graham 2016). Such a feature may be apparent in NGC 4424 (Cortés et al. 2006, see their Figure 2), where, interestingly, there are also signs that this structure forms the inner half of a figure-of-eight pattern, such as that more clearly seen in NGC 4429 (Frei et al. 1996; Baillard et al. 2011; Cappellari et al. 2011, their Figure 6). In passing, we speculate that NGC 4429 may, therefore, represent a more evolved state of NGC 4424. NGC 4608 (Cappellari et al. 2011) may offer a more face-on representation of NGC 4429. If so, then the figure-of-eight pattern may arise from an X-shaped pseudobulge coupled with the ansae/ring at the end of the original bar.

At $6 \times 10^{10} M_{\odot}$ (Licquia & Newman 2015), the Milky Way has a stellar mass some six times bigger than NGC 4424, and a clear X/P pseudobulge (Ciambur et al. 2017, and references therein). This pseudobulge, which peaks at roughly half the length of the bar, likely formed from perturbations to the bar due to by minor fly-bys (Kumar et al. 2021) or minor mergers which also contribute to the classical bulge (Nataf 2017; Zoccali et al. 2018). If six minor merger events have brought in six $10^5 M_{\odot}$ black holes, one might (naively) expect a central black hole with a minimum mass of $0.6 \times 10^6 M_{\odot}$, with gas fuelling and stellar capture perhaps increasing this to the observed value of $4 \times 10^6 M_{\odot}$ (Boehle et al. 2016). The zoom-in hydrodynamical simulation of (Bonoli et al. 2016) supports such growth by infall and black hole merging. It would also explain the tentative suggestions of IMBHs infalling/wandering in the Milky Way (Takekawa et al. 2020, and references therein).

6. SUMMARY

We have discovered, in *HST* imaging, a red, elongated star cluster located ~ 400 pc ($\sim 5''$), in projection, from the center of the post-merger galaxy NGC 4424. This may be the remnants of the infalling galaxy responsible for the known, past minor-merger event that disturbed NGC 4424. The star cluster, referred to as Nikhuli, is stretched in the direction of NGC 4424’s center, and could be the nuclear star cluster of the captured galaxy.

Based on the $3 \times 10^6 M_{\odot}$ stellar mass of Nikhuli, we used the $M_{\text{bh}}-M_{\text{nc}}$ scaling relation to predict that it

may harbour an intermediate-mass black hole of $7 \times 10^4 M_\odot$, although this estimate has a considerable 1.6 dex of uncertainty. Interestingly, Nikhuli corresponds spatially with a *CXO* X-ray point-source having $L_X \equiv L_{0.5-10\text{ keV}} = 0.7 \times 10^{39} \text{ erg s}^{-1}$ for a photon index $\Gamma = 1.7$. While this source may be a super-Eddington stellar-mass black hole, we argue that it is more likely to be a sub-Eddington massive black hole.

Based on the stellar mass and velocity dispersion of NGC 4424, it is expected to possess an intermediate-mass black hole with $\log M_{\text{bh}}/M_\odot = 4.9 \pm 0.6$. While the X-ray point-source in Nikhuli is highly unlikely to be a high-mass X-ray binary, we estimate that there is a 7% chance that it may be a low-mass X-ray binary *if* the formation efficiency of LMXBs in nuclear star clusters is 1000 times greater than that of a galaxy’s field stars. On the other hand, given that nuclear star clusters and massive black holes are known to regularly coexist, Nikhuli may be the delivery vehicle for seeding a, or at least helping to grow the, massive black hole in NGC 4424. At the same time, Nikhuli’s now disrupted host galaxy may have been sewn into the fabric of NGC 4424, contributing to the build up of the stellar halo or a classical bulge depending on how far the stars penetrate.

We plan to search for more such hidden structures, like Nikhuli, in 74 other Virgo cluster spiral galaxies imaged by *CXO* (Soria et al. 2021). To date, a lot of the tidal stream discoveries have occurred in the halos of galaxies. Our galaxy capture-and-subtract process will hopefully enable one to better probe the inner regions. In particular, we intend to cross-match any new discoveries with the off-center ULXs identified by (Soria et al. 2021). This may provide a statistical argument for how important minor merging could be as either a black hole seeding or growth mechanism for late-type spiral galaxies.

ACKNOWLEDGMENTS

This research was supported under the Australian Research Council’s funding scheme DP17012923 and is based upon work supported by Tamkeen under the NYU Abu Dhabi Research Institute grant CAP³. RS warmly thanks Curtin University for their hospitality during the planning stage of this project. Support for this work was provided by the National Aeronautics and Space Administration through Chandra Award Number LP18620568 issued by the Chandra X-ray Center, which is operated by the Smithsonian Astrophysical Observatory for and on behalf of the National Aeronautics Space Administration under contract NAS8-03060. Data underlying this article are available in the Chandra Data Archive (CDA: <https://cxc.harvard.edu/cda/>), and the Next Generation Virgo Cluster Survey website (<https://www.cfht.hawaii.edu/Science/NGVS/>). Based on observations made with the NASA/ESA Hubble Space Telescope, and obtained from the Hubble Legacy Archive, which is a collaboration between the Space Telescope Science Institute (STScI/NASA), the Space Telescope European Coordinating Facility (ST-ECF/ESA) and the Canadian Astronomy Data Center (CADC/NRC/CSA). This research has made use of NASA’s Astrophysics Data System (ADS) Bibliographic Services and of the NASA/IPAC Extragalactic Database (NED), which is operated by the Jet Propulsion Laboratory, California Institute of Technology, under contract with NASA.

Software: IRAF (Tody 1986, 1993), *Isfit/Cmodel* (Ciambur 2015), PROFILER (Ciambur 2016), XSPEC (v12.11.0: Arnaud 1996), CIAO (v4.12: Fruscione et al. 2006), SAS (v17.0.0: Gabriel et al. 2004), ds9 (Joye & Mandel 2003).

REFERENCES

- Ahn, C. P., Seth, A. C., den Brok, M., et al. 2017, *ApJ*, 839, 72, doi: [10.3847/1538-4357/aa6972](https://doi.org/10.3847/1538-4357/aa6972)
- Alexander, T., & Natarajan, P. 2014, *Science*, 345, 1330, doi: [10.1126/science.1251053](https://doi.org/10.1126/science.1251053)
- Alzate, J. A., Lora, V., Bruzual, G., Lomelí-Núñez, L., & Cervantes Sodi, B. 2021, *MNRAS*, 505, 2074, doi: [10.1093/mnras/stab1322](https://doi.org/10.1093/mnras/stab1322)
- Arca-Sedda, M., & Capuzzo-Dolcetta, R. 2014a, *ApJ*, 785, 51, doi: [10.1088/0004-637X/785/1/51](https://doi.org/10.1088/0004-637X/785/1/51)
- . 2014b, *MNRAS*, 444, 3738, doi: [10.1093/mnras/stu1683](https://doi.org/10.1093/mnras/stu1683)
- Arca-Sedda, M., Capuzzo-Dolcetta, R., Antonini, F., & Seth, A. 2015, *ApJ*, 806, 220, doi: [10.1088/0004-637X/806/2/220](https://doi.org/10.1088/0004-637X/806/2/220)
- Arnaud, K. A. 1996, in *Astronomical Society of the Pacific Conference Series*, Vol. 101, *Astronomical Data Analysis Software and Systems V*, ed. G. H. Jacoby & J. Barnes, 17
- Arp, H. 1964, *ApJ*, 139, 1045, doi: [10.1086/147844](https://doi.org/10.1086/147844)
- Askar, A., Davies, M. B., & Church, R. P. 2021, *MNRAS*, 502, 2682, doi: [10.1093/mnras/stab113](https://doi.org/10.1093/mnras/stab113)
- Athanassoula, E. 1992, *MNRAS*, 259, 345, doi: [10.1093/mnras/259.2.345](https://doi.org/10.1093/mnras/259.2.345)
- . 2005, *MNRAS*, 358, 1477, doi: [10.1111/j.1365-2966.2005.08872.x](https://doi.org/10.1111/j.1365-2966.2005.08872.x)
- Baade, W., & Minkowski, R. 1954, *ApJ*, 119, 206, doi: [10.1086/145812](https://doi.org/10.1086/145812)

- Bachetti, M., Harrison, F. A., Walton, D. J., et al. 2014, *Nature*, 514, 202, doi: [10.1038/nature13791](https://doi.org/10.1038/nature13791)
- Baillard, A., Bertin, E., de Lapparent, V., et al. 2011, *A&A*, 532, A74, doi: [10.1051/0004-6361/201016423](https://doi.org/10.1051/0004-6361/201016423)
- Bajaj, V. 2019, WFC3/IR Photometric Repeatability, Space Telescope WFC Instrument Science Report
- Balcells, M., Graham, A. W., Domínguez-Palmero, L., & Peletier, R. F. 2003, *ApJL*, 582, L79, doi: [10.1086/367783](https://doi.org/10.1086/367783)
- Balcells, M., Graham, A. W., & Peletier, R. F. 2007, *ApJ*, 665, 1084, doi: [10.1086/519752](https://doi.org/10.1086/519752)
- Banik, U., & van den Bosch, F. C. 2021, *ApJ*, 912, 43, doi: [10.3847/1538-4357/abeb6d](https://doi.org/10.3847/1538-4357/abeb6d)
- Baranov, A. S., & Batrakov, Y. V. 1974, *Soviet Ast.*, 18, 180
- Barausse, E. 2012, *MNRAS*, 423, 2533, doi: [10.1111/j.1365-2966.2012.21057.x](https://doi.org/10.1111/j.1365-2966.2012.21057.x)
- Bardeen, J. M. 1975, in *IAU Symposium*, Vol. 69, *Dynamics of the Solar Systems*, ed. A. Hayli (Dordrecht; Boston: D. Reidel Pub. Co.), 297
- Barrows, R. S., Mezcuca, M., & Comerford, J. M. 2019, *ApJ*, 882, 181, doi: [10.3847/1538-4357/ab338a](https://doi.org/10.3847/1538-4357/ab338a)
- Baumgardt, H., Hopman, C., Portegies Zwart, S., & Makino, J. 2006, *MNRAS*, 372, 467, doi: [10.1111/j.1365-2966.2006.10885.x](https://doi.org/10.1111/j.1365-2966.2006.10885.x)
- Baumgardt, H., He, C., Sweet, S. M., et al. 2019, *MNRAS*, 488, 5340, doi: [10.1093/mnras/stz2060](https://doi.org/10.1093/mnras/stz2060)
- Becker, W., Swartz, D. A., Pavlov, G. G., et al. 2003, *ApJ*, 594, 798, doi: [10.1086/376967](https://doi.org/10.1086/376967)
- Bekki, K. 2010, *MNRAS*, 401, 2753, doi: [10.1111/j.1365-2966.2009.15874.x](https://doi.org/10.1111/j.1365-2966.2009.15874.x)
- Bekki, K., Couch, W. J., & Drinkwater, M. J. 2001, *ApJL*, 552, L105, doi: [10.1086/320339](https://doi.org/10.1086/320339)
- Bekki, K., Couch, W. J., Drinkwater, M. J., & Shioya, Y. 2003, *MNRAS*, 344, 399, doi: [10.1046/j.1365-8711.2003.06916.x](https://doi.org/10.1046/j.1365-8711.2003.06916.x)
- Bekki, K., & Freeman, K. C. 2003, *MNRAS*, 346, L11, doi: [10.1046/j.1365-2966.2003.07275.x](https://doi.org/10.1046/j.1365-2966.2003.07275.x)
- Bellovary, J. M., Cleary, C. E., Munshi, F., et al. 2019, *MNRAS*, 482, 2913, doi: [10.1093/mnras/sty2842](https://doi.org/10.1093/mnras/sty2842)
- Bellovary, J. M., Governato, F., Quinn, T. R., et al. 2010, *ApJL*, 721, L148, doi: [10.1088/2041-8205/721/2/L148](https://doi.org/10.1088/2041-8205/721/2/L148)
- Bellovary, J. M., Hayoune, S., Chafra, K., et al. 2021, *MNRAS*, 505, 5129, doi: [10.1093/mnras/stab1665](https://doi.org/10.1093/mnras/stab1665)
- Belokurov, V., Erkal, D., Evans, N. W., Koposov, S. E., & Deason, A. J. 2018, *MNRAS*, 478, 611, doi: [10.1093/mnras/sty982](https://doi.org/10.1093/mnras/sty982)
- Belokurov, V., Zucker, D. B., Evans, N. W., et al. 2006, *ApJL*, 642, L137, doi: [10.1086/504797](https://doi.org/10.1086/504797)
- Binggeli, B., Barazza, F., & Jerjen, H. 2000, *A&A*, 359, 447
- Binney, J., & Tremaine, S. 1987, *Galactic dynamics* ((Princeton, NJ: Princeton Univ. Press))
- Blakeslee, J. P., & Tonry, J. L. 1992, *AJ*, 103, 1457, doi: [10.1086/116160](https://doi.org/10.1086/116160)
- Blecha, L., & Loeb, A. 2008, *MNRAS*, 390, 1311, doi: [10.1111/j.1365-2966.2008.13790.x](https://doi.org/10.1111/j.1365-2966.2008.13790.x)
- Boehle, A., Ghez, A. M., Schödel, R., et al. 2016, *ApJ*, 830, 17, doi: [10.3847/0004-637X/830/1/17](https://doi.org/10.3847/0004-637X/830/1/17)
- Böker, T., Laine, S., van der Marel, R. P., et al. 2002, *AJ*, 123, 1389, doi: [10.1086/339025](https://doi.org/10.1086/339025)
- Boldrini, P., Mohayaee, R., & Silk, J. 2020, *MNRAS*, 495, L12, doi: [10.1093/mnras/rlaa043](https://doi.org/10.1093/mnras/rlaa043)
- Bonaca, A., Naidu, R. P., Conroy, C., et al. 2021, *ApJL*, 909, L26, doi: [10.3847/2041-8213/abeaa9](https://doi.org/10.3847/2041-8213/abeaa9)
- Bonfini, P., & Graham, A. W. 2016, *ApJ*, 829, 81, doi: [10.3847/0004-637X/829/2/81](https://doi.org/10.3847/0004-637X/829/2/81)
- Bonoli, S., Mayer, L., Kazantzidis, S., et al. 2016, *MNRAS*, 459, 2603, doi: [10.1093/mnras/stw694](https://doi.org/10.1093/mnras/stw694)
- Bortolas, E., Bonetti, M., Dotti, M., et al. 2021, The role of bars on the dynamical-friction driven inspiral of massive perturbers. <https://arxiv.org/abs/2103.07486>
- Boselli, A., Fossati, M., Gavazzi, G., et al. 2015, *A&A*, 579, A102, doi: [10.1051/0004-6361/201525712](https://doi.org/10.1051/0004-6361/201525712)
- Boselli, A., Fossati, M., Consolandi, G., et al. 2018, *A&A*, 620, A164, doi: [10.1051/0004-6361/201833914](https://doi.org/10.1051/0004-6361/201833914)
- Busch, G., Zuther, J., Valencia-S., M., et al. 2014, *A&A*, 561, A140, doi: [10.1051/0004-6361/201322486](https://doi.org/10.1051/0004-6361/201322486)
- Cappellari, M., Emsellem, E., Krajnović, D., et al. 2011, *MNRAS*, 413, 813, doi: [10.1111/j.1365-2966.2010.18174.x](https://doi.org/10.1111/j.1365-2966.2010.18174.x)
- Carollo, C. M. 1999, *ApJ*, 523, 566, doi: [10.1086/307753](https://doi.org/10.1086/307753)
- Cash, W. 1979, *ApJ*, 228, 939, doi: [10.1086/156922](https://doi.org/10.1086/156922)
- Chandrasekhar, S., & von Neumann, J. 1943, *ApJ*, 97, 1, doi: [10.1086/144487](https://doi.org/10.1086/144487)
- Chang, J., Yuan, Z., Xue, X.-X., et al. 2020, *ApJ*, 905, 100, doi: [10.3847/1538-4357/abc338](https://doi.org/10.3847/1538-4357/abc338)
- Chen, N., Ni, Y., Tremmel, M., et al. 2021, Dynamical Friction Modeling of Massive Black Holes in Cosmological Simulations and Effects on Merger Rate Predictions. <https://arxiv.org/abs/2104.00021>
- Ciambur, B. C. 2015, *ApJ*, 810, 120, doi: [10.1088/0004-637X/810/2/120](https://doi.org/10.1088/0004-637X/810/2/120)
- . 2016, *PASA*, 33, e062, doi: [10.1017/pasa.2016.60](https://doi.org/10.1017/pasa.2016.60)
- Ciambur, B. C., & Graham, A. W. 2016, *MNRAS*, 459, 1276, doi: [10.1093/mnras/stw759](https://doi.org/10.1093/mnras/stw759)
- Ciambur, B. C., Graham, A. W., & Bland-Hawthorn, J. 2017, *MNRAS*, 471, 3988, doi: [10.1093/mnras/stx1823](https://doi.org/10.1093/mnras/stx1823)
- Combes, F., Debbasch, F., Friedli, D., & Pfenniger, D. 1990, *A&A*, 233, 82
- Combes, F., & Sanders, R. H. 1981, *A&A*, 96, 164

- Corral, A., Della Ceca, R., Caccianiga, A., et al. 2011, *A&A*, 530, A42, doi: [10.1051/0004-6361/201015227](https://doi.org/10.1051/0004-6361/201015227)
- Cortés, J. R., Kenney, J. D. P., & Hardy, E. 2006, *AJ*, 131, 747, doi: [10.1086/499075](https://doi.org/10.1086/499075)
- . 2008, *ApJ*, 683, 78, doi: [10.1086/588604](https://doi.org/10.1086/588604)
- Côté, P., Piatek, S., Ferrarese, L., et al. 2006, *ApJS*, 165, 57, doi: [10.1086/504042](https://doi.org/10.1086/504042)
- Davis, B. L., Graham, A. W., & Cameron, E. 2018, *ApJ*, 869, 113, doi: [10.3847/1538-4357/aae820](https://doi.org/10.3847/1538-4357/aae820)
- . 2019, *ApJ*, 873, 85, doi: [10.3847/1538-4357/aaf3b8](https://doi.org/10.3847/1538-4357/aaf3b8)
- Davis, B. L., Graham, A. W., & Seigar, M. S. 2017, *MNRAS*, 471, 2187, doi: [10.1093/mnras/stx1794](https://doi.org/10.1093/mnras/stx1794)
- de Vaucouleurs, G., de Vaucouleurs, A., Corwin, Herold G., J., et al. 1991, *Third Reference Catalogue of Bright Galaxies* (Springer, New York)
- Drlica-Wagner, A., Bechtol, K., Rykoff, E. S., et al. 2015, *ApJ*, 813, 109, doi: [10.1088/0004-637X/813/2/109](https://doi.org/10.1088/0004-637X/813/2/109)
- Düchting, N. 2004, *PhRvD*, 70, 064015, doi: [10.1103/PhysRevD.70.064015](https://doi.org/10.1103/PhysRevD.70.064015)
- Earnshaw, H. P., Roberts, T. P., Middleton, M. J., Walton, D. J., & Mateos, S. 2019, *MNRAS*, 483, 5554, doi: [10.1093/mnras/sty3403](https://doi.org/10.1093/mnras/sty3403)
- Farrell, S. A., Webb, N. A., Barret, D., Godet, O., & Rodrigues, J. M. 2009, *Nature*, 460, 73, doi: [10.1038/nature08083](https://doi.org/10.1038/nature08083)
- Feng, H., & Soria, R. 2011, *New Astronomy Reviews*, 55, 166, doi: [10.1016/j.newar.2011.08.002](https://doi.org/10.1016/j.newar.2011.08.002)
- Ferguson, P., Shipp, N., Drlica-Wagner, A., et al. 2021, *DELVE-ing into the Jet: a thin stellar stream on a retrograde orbit at 30 kpc.* <https://arxiv.org/abs/2104.11755>
- Ferrarese, L., Côté, P., Jordán, A., et al. 2006, *ApJS*, 164, 334, doi: [10.1086/501350](https://doi.org/10.1086/501350)
- Ferrarese, L., Côté, P., Cuilland re, J.-C., et al. 2012, *ApJS*, 200, 4, doi: [10.1088/0067-0049/200/1/4](https://doi.org/10.1088/0067-0049/200/1/4)
- Ferrarese, L., Côté, P., Sánchez-Janssen, R., et al. 2016, *ApJ*, 824, 10, doi: [10.3847/0004-637X/824/1/10](https://doi.org/10.3847/0004-637X/824/1/10)
- Forbes, D. A., Beasley, M. A., Bekki, K., Brodie, J. P., & Strader, J. 2003, *Science*, 301, 1217, doi: [10.1126/science.1089237](https://doi.org/10.1126/science.1089237)
- Forbes, D. A., Franx, M., & Illingworth, G. D. 1995, *AJ*, 109, 1988, doi: [10.1086/117425](https://doi.org/10.1086/117425)
- Foster, C., Lux, H., Romanowsky, A. J., et al. 2014, *MNRAS*, 442, 3544, doi: [10.1093/mnras/stu1074](https://doi.org/10.1093/mnras/stu1074)
- Fragos, T., Lehmer, B., Tremmel, M., et al. 2013, *ApJ*, 764, 41, doi: [10.1088/0004-637X/764/1/41](https://doi.org/10.1088/0004-637X/764/1/41)
- Franx, M., Illingworth, G., & Heckman, T. 1989, *ApJ*, 344, 613, doi: [10.1086/167830](https://doi.org/10.1086/167830)
- Freeman, K. C. 1993, in *Astronomical Society of the Pacific Conference Series*, Vol. 48, *The globular clusters-galaxy connection*, ed. G. H. Smith & J. P. Brodie, 608
- Frei, Z., Guhathakurta, P., Gunn, J. E., & Tyson, J. A. 1996, *AJ*, 111, 174, doi: [10.1086/117771](https://doi.org/10.1086/117771)
- Fruscione, A., McDowell, J. C., Allen, G. E., et al. 2006, in *Society of Photo-Optical Instrumentation Engineers (SPIE) Conference Series*, Vol. 6270, *Society of Photo-Optical Instrumentation Engineers (SPIE) Conference Series*, 62701V, doi: [10.1117/12.671760](https://doi.org/10.1117/12.671760)
- Gabriel, C., Denby, M., Fyfe, D. J., et al. 2004, in *Astronomical Society of the Pacific Conference Series*, Vol. 314, *Astronomical Data Analysis Software and Systems (ADASS) XIII*, ed. F. Ochsenbein, M. G. Allen, & D. Egret, 759
- Gallo, E., Treu, T., Marshall, P. J., et al. 2010, *ApJ*, 714, 25, doi: [10.1088/0004-637X/714/1/25](https://doi.org/10.1088/0004-637X/714/1/25)
- Gao, Y., Wang, Q. D., Appleton, P. N., & Lucas, R. A. 2003, *ApJL*, 596, L171, doi: [10.1086/379598](https://doi.org/10.1086/379598)
- Gavazzi, G., Boselli, A., Donati, A., Franzetti, P., & Scodreggio, M. 2003, *A&A*, 400, 451, doi: [10.1051/0004-6361:20030026](https://doi.org/10.1051/0004-6361:20030026)
- Ghosh, P., & White, N. E. 2001, *ApJL*, 559, L97, doi: [10.1086/323641](https://doi.org/10.1086/323641)
- Goerdt, T., Moore, B., Read, J. I., Stadel, J., & Zemp, M. 2006, *MNRAS*, 368, 1073, doi: [10.1111/j.1365-2966.2006.10182.x](https://doi.org/10.1111/j.1365-2966.2006.10182.x)
- Gordon, K. D., Bailin, J., Engelbracht, C. W., et al. 2006, *ApJL*, 638, L87, doi: [10.1086/501046](https://doi.org/10.1086/501046)
- Graham, A. W. 2002, *ApJL*, 568, L13, doi: [10.1086/340274](https://doi.org/10.1086/340274)
- . 2020, *MNRAS*, 492, 3263, doi: [10.1093/mnras/stz3547](https://doi.org/10.1093/mnras/stz3547)
- Graham, A. W., Colless, M. M., Busarello, G., Zaggia, S., & Longo, G. 1998, *A&AS*, 133, 325, doi: [10.1051/aas:1998325](https://doi.org/10.1051/aas:1998325)
- Graham, A. W., Dullo, B. T., & Savorgnan, G. A. D. 2015, *ApJ*, 804, 32, doi: [10.1088/0004-637X/804/1/32](https://doi.org/10.1088/0004-637X/804/1/32)
- Graham, A. W., & Guzmán, R. 2003, *AJ*, 125, 2936, doi: [10.1086/374992](https://doi.org/10.1086/374992)
- Graham, A. W., Merritt, D., Moore, B., Diemand, J., & Terzić, B. 2006, *AJ*, 132, 2701, doi: [10.1086/508990](https://doi.org/10.1086/508990)
- Graham, A. W., & Soria, R. 2019, *MNRAS*, 484, 794, doi: [10.1093/mnras/sty3398](https://doi.org/10.1093/mnras/sty3398)
- Graham, A. W., Soria, R., & Davis, B. L. 2019, *MNRAS*, 484, 814, doi: [10.1093/mnras/sty3068](https://doi.org/10.1093/mnras/sty3068)
- Graham, A. W., Soria, R., Davis, B. L., et al. 2021, *ApJ*, in press
- Graham, A. W., & Spitler, L. R. 2009, *MNRAS*, 397, 2148, doi: [10.1111/j.1365-2966.2009.15118.x](https://doi.org/10.1111/j.1365-2966.2009.15118.x)
- Graham, A. W., & Worley, C. C. 2008, *MNRAS*, 388, 1708, doi: [10.1111/j.1365-2966.2008.13506.x](https://doi.org/10.1111/j.1365-2966.2008.13506.x)

- Graur, O., Zurek, D., Shara, M. M., et al. 2016, *ApJ*, 819, 31, doi: [10.3847/0004-637X/819/1/31](https://doi.org/10.3847/0004-637X/819/1/31)
- Grimm, H. J., Gilfanov, M., & Sunyaev, R. 2003, *MNRAS*, 339, 793, doi: [10.1046/j.1365-8711.2003.06224.x](https://doi.org/10.1046/j.1365-8711.2003.06224.x)
- Hansen, T. T., Ji, A. P., Da Costa, G. S., et al. 2021, *ApJ*, 915, 103, doi: [10.3847/1538-4357/abfc54](https://doi.org/10.3847/1538-4357/abfc54)
- Hatt, D., Freedman, W. L., Madore, B. F., et al. 2018, *ApJ*, 861, 104, doi: [10.3847/1538-4357/aac9cc](https://doi.org/10.3847/1538-4357/aac9cc)
- Hau, G. K. T., Carter, D., & Balcells, M. 1999, *MNRAS*, 306, 437, doi: [10.1046/j.1365-8711.1999.02526.x](https://doi.org/10.1046/j.1365-8711.1999.02526.x)
- Helmi, A., Babusiaux, C., Koppelman, H. H., et al. 2018, *Nature*, 563, 85, doi: [10.1038/s41586-018-0625-x](https://doi.org/10.1038/s41586-018-0625-x)
- HI4PI Collaboration, Ben Bekhti, N., Flöer, L., et al. 2016, *A&A*, 594, A116, doi: [10.1051/0004-6361/201629178](https://doi.org/10.1051/0004-6361/201629178)
- Ho, L. C., Greene, J. E., Filippenko, A. V., & Sargent, W. L. W. 2009, *ApJS*, 183, 1, doi: [10.1088/0067-0049/183/1/1](https://doi.org/10.1088/0067-0049/183/1/1)
- Hogg, J. D., Blecha, L., Reynolds, C. S., Smith, K. L., & Winter, L. M. 2021, *MNRAS*, 503, 1688, doi: [10.1093/mnras/stab576](https://doi.org/10.1093/mnras/stab576)
- Hohl, F. 1975, in *Dynamics of the Solar Systems*, ed. A. Hayli, Vol. 69 (Dordrecht; Boston: D. Reidel Pub. Co.), 349
- Holley-Bockelmann, K., Gültekin, K., Shoemaker, D., & Yunes, N. 2008, *ApJ*, 686, 829, doi: [10.1086/591218](https://doi.org/10.1086/591218)
- Hut, P., McMillan, S., Goodman, J., et al. 1992, *PASP*, 104, 981, doi: [10.1086/133085](https://doi.org/10.1086/133085)
- Ibata, R. A., Bellazzini, M., Malhan, K., Martin, N., & Bianchini, P. 2019a, *Nature Astronomy*, 3, 667, doi: [10.1038/s41550-019-0751-x](https://doi.org/10.1038/s41550-019-0751-x)
- Ibata, R. A., Gilmore, G., & Irwin, M. J. 1994, *Nature*, 370, 194, doi: [10.1038/370194a0](https://doi.org/10.1038/370194a0)
- Ibata, R. A., Malhan, K., & Martin, N. F. 2019b, *ApJ*, 872, 152, doi: [10.3847/1538-4357/ab0080](https://doi.org/10.3847/1538-4357/ab0080)
- Inoue, S. 2009, *MNRAS*, 397, 709, doi: [10.1111/j.1365-2966.2009.15066.x](https://doi.org/10.1111/j.1365-2966.2009.15066.x)
- . 2011, *MNRAS*, 416, 1181, doi: [10.1111/j.1365-2966.2011.19122.x](https://doi.org/10.1111/j.1365-2966.2011.19122.x)
- Jenner, D. C. 1974, *ApJ*, 191, 55, doi: [10.1086/152939](https://doi.org/10.1086/152939)
- Jordán, A., Côté, P., Blakeslee, J. P., et al. 2005, *ApJ*, 634, 1002, doi: [10.1086/497092](https://doi.org/10.1086/497092)
- Joye, W. A., & Mandel, E. 2003, in *Astronomical Society of the Pacific Conference Series*, Vol. 295, *Astronomical Data Analysis Software and Systems XII*, ed. H. E. Payne, R. I. Jedrzejewski, & R. N. Hook, 489
- Kaaret, P., Feng, H., & Roberts, T. P. 2017, *ARA&A*, 55, 303, doi: [10.1146/annurev-astro-091916-055259](https://doi.org/10.1146/annurev-astro-091916-055259)
- Kenney, J. D. P., Koopmann, R. A., Rubin, V. C., & Young, J. S. 1996, *AJ*, 111, 152, doi: [10.1086/117768](https://doi.org/10.1086/117768)
- Kim, D. W., Fabbiano, G., Ivanova, N., et al. 2013, *ApJ*, 764, 98, doi: [10.1088/0004-637X/764/1/98](https://doi.org/10.1088/0004-637X/764/1/98)
- Kim, M., López, K. M., Jonker, P. G., Ho, L. C., & Im, M. 2020, *MNRAS*, 493, L76, doi: [10.1093/mnrasl/slaa011](https://doi.org/10.1093/mnrasl/slaa011)
- Kim, M., Ho, L. C., Wang, J., et al. 2015, *ApJ*, 814, 8, doi: [10.1088/0004-637X/814/1/8](https://doi.org/10.1088/0004-637X/814/1/8)
- Koekemoer, A. M., Ellis, R. S., McLure, R. J., et al. 2013, *ApJS*, 209, 3, doi: [10.1088/0067-0049/209/1/3](https://doi.org/10.1088/0067-0049/209/1/3)
- Komossa, S. 2015, *Journal of High Energy Astrophysics*, 7, 148, doi: [10.1016/j.jheap.2015.04.006](https://doi.org/10.1016/j.jheap.2015.04.006)
- Komossa, S., & Merritt, D. 2008, *ApJL*, 689, L89, doi: [10.1086/595883](https://doi.org/10.1086/595883)
- Koposov, S. E., Belokurov, V., Zucker, D. B., et al. 2015, *MNRAS*, 446, 3110, doi: [10.1093/mnras/stu2263](https://doi.org/10.1093/mnras/stu2263)
- Kormendy, J., Drory, N., Bender, R., & Cornell, M. E. 2010, *ApJ*, 723, 54, doi: [10.1088/0004-637X/723/1/54](https://doi.org/10.1088/0004-637X/723/1/54)
- Korovnikovskii, I. P., Petrosian, A. R., Saakian, K. A., & Khachikian, E. E. 1981, *Astrofizika*, 17, 231
- Koushiappas, S. M., Bullock, J. S., & Dekel, A. 2004, *MNRAS*, 354, 292, doi: [10.1111/j.1365-2966.2004.08190.x](https://doi.org/10.1111/j.1365-2966.2004.08190.x)
- Kozhurina-Platais, V., & Baggett, S. 2020, *WFC3 IR sensitivity over time*, *Space Telescope WFC Instrument Science Report*
- Kraft, R. P., Burrows, D. N., & Nousek, J. A. 1991, *ApJ*, 374, 344, doi: [10.1086/170124](https://doi.org/10.1086/170124)
- Kubota, A., Tanaka, Y., Makishima, K., et al. 1998, *PASJ*, 50, 667, doi: [10.1093/pasj/50.6.667](https://doi.org/10.1093/pasj/50.6.667)
- Kumar, A., Das, M., & Kataria, S. K. 2021, *MNRAS*, 506, 98, doi: [10.1093/mnras/stab1742](https://doi.org/10.1093/mnras/stab1742)
- Lehmer, B. D., Eufrasio, R. T., Tzanavaris, P., et al. 2019, *ApJS*, 243, 3, doi: [10.3847/1538-4365/ab22a8](https://doi.org/10.3847/1538-4365/ab22a8)
- Lehmer, B. D., Ferrell, A. P., Doore, K., et al. 2020, *ApJS*, 248, 31, doi: [10.3847/1538-4365/ab9175](https://doi.org/10.3847/1538-4365/ab9175)
- Licquia, T. C., & Newman, J. A. 2015, *ApJ*, 806, 96, doi: [10.1088/0004-637X/806/1/96](https://doi.org/10.1088/0004-637X/806/1/96)
- Lin, D., Strader, J., Carrasco, E. R., et al. 2018, *Nature Astronomy*, 2, 656, doi: [10.1038/s41550-018-0493-1](https://doi.org/10.1038/s41550-018-0493-1)
- Lindblad, B. 1927, *MNRAS*, 87, 420, doi: [10.1093/mnras/87.5.420](https://doi.org/10.1093/mnras/87.5.420)
- Liu, C., Peng, E. W., Toloba, E., et al. 2015, *ApJL*, 812, L2, doi: [10.1088/2041-8205/812/1/L2](https://doi.org/10.1088/2041-8205/812/1/L2)
- Lotz, J. M., Telford, R., Ferguson, H. C., et al. 2001, *ApJ*, 552, 572, doi: [10.1086/320545](https://doi.org/10.1086/320545)
- Ma, L., Hopkins, P. F., Ma, X., et al. 2021, *MNRAS*, 508, 1973, doi: [10.1093/mnras/stab2713](https://doi.org/10.1093/mnras/stab2713)
- Maccarone, T. J., Kundu, A., & Zepf, S. E. 2003, *ApJ*, 586, 814, doi: [10.1086/367886](https://doi.org/10.1086/367886)
- Malhan, K., Yuan, Z., Ibata, R. A., et al. 2021, *ApJ*, 920, 51, doi: [10.3847/1538-4357/ac1675](https://doi.org/10.3847/1538-4357/ac1675)

- Mapelli, M., Zampieri, L., & Mayer, L. 2012, MNRAS, 423, 1309, doi: [10.1111/j.1365-2966.2012.20955.x](https://doi.org/10.1111/j.1365-2966.2012.20955.x)
- Martin, N. F., Ibata, R. A., Rich, R. M., et al. 2014, ApJ, 787, 19, doi: [10.1088/0004-637X/787/1/19](https://doi.org/10.1088/0004-637X/787/1/19)
- Martínez-Delgado, D., Gabany, R. J., Crawford, K., et al. 2010, AJ, 140, 962, doi: [10.1088/0004-6256/140/4/962](https://doi.org/10.1088/0004-6256/140/4/962)
- Martínez-Delgado, D., Cooper, A. P., Roman, J., et al. 2021, Hidden Depths in the Local Universe: the Stellar Stream Legacy Survey. <https://arxiv.org/abs/2104.06071>
- Merritt, D., Ferrarese, L., & Joseph, C. L. 2001, Science, 293, 1116, doi: [10.1126/science.1063896](https://doi.org/10.1126/science.1063896)
- Merritt, D., & Milosavljević, M. 2005, Living Reviews in Relativity, 8, 8, doi: [10.12942/lrr-2005-8](https://doi.org/10.12942/lrr-2005-8)
- Mezcua, M., Roberts, T. P., Lobanov, A. P., & Sutton, A. D. 2015, MNRAS, 448, 1893, doi: [10.1093/mnras/stv143](https://doi.org/10.1093/mnras/stv143)
- Milosavljević, M. 2004, ApJL, 605, L13, doi: [10.1086/420696](https://doi.org/10.1086/420696)
- Mineo, S., Gilfanov, M., & Sunyaev, R. 2012, MNRAS, 426, 1870, doi: [10.1111/j.1365-2966.2012.21831.x](https://doi.org/10.1111/j.1365-2966.2012.21831.x)
- Miskolczi, A., Bomans, D. J., & Dettmar, R. J. 2011, A&A, 536, A66, doi: [10.1051/0004-6361/201116716](https://doi.org/10.1051/0004-6361/201116716)
- Molina, M., Bassani, L., Malizia, A., et al. 2009, MNRAS, 399, 1293, doi: [10.1111/j.1365-2966.2009.15257.x](https://doi.org/10.1111/j.1365-2966.2009.15257.x)
- Morales, G., Martínez-Delgado, D., Grebel, E. K., et al. 2018, A&A, 614, A143, doi: [10.1051/0004-6361/201732271](https://doi.org/10.1051/0004-6361/201732271)
- Morton, B., Khochfar, S., & Oñorbe, J. 2021, Gaseous Dynamical Friction: A Challenge to Modern Hydrodynamical Schemes. <https://arxiv.org/abs/2103.15848>
- Munari, U., Henden, A., Belligoli, R., et al. 2013, New Astronomy, 20, 30, doi: [10.1016/j.newast.2012.09.003](https://doi.org/10.1016/j.newast.2012.09.003)
- Nataf, D. M. 2017, PASA, 34, e041, doi: [10.1017/pasa.2017.32](https://doi.org/10.1017/pasa.2017.32)
- Navarro, J. F., Frenk, C. S., & White, S. D. M. 1996, ApJ, 462, 563, doi: [10.1086/177173](https://doi.org/10.1086/177173)
- Newberg, H. J. 2016, in Astrophysics and Space Science Library, Vol. 420, Tidal Streams in the Local Group and Beyond, ed. H. J. Newberg & J. L. Carlin (Springer International Publishing), 1–29, doi: [10.1007/978-3-319-19336-6_1](https://doi.org/10.1007/978-3-319-19336-6_1)
- Oh, K. S., & Lin, D. N. C. 2000, ApJ, 543, 620, doi: [10.1086/317118](https://doi.org/10.1086/317118)
- Owen, R. A., & Warwick, R. S. 2009, MNRAS, 394, 1741, doi: [10.1111/j.1365-2966.2009.14464.x](https://doi.org/10.1111/j.1365-2966.2009.14464.x)
- Paudel, S., Lisker, T., & Kuntschner, H. 2011, MNRAS, 413, 1764, doi: [10.1111/j.1365-2966.2011.18256.x](https://doi.org/10.1111/j.1365-2966.2011.18256.x)
- Petrosian, A. R., Saakian, K. A., & Khachikian, E. E. 1978, Astrofizika, 14, 69
- Petts, J. A., Gualandris, A., & Read, J. I. 2015, MNRAS, 454, 3778, doi: [10.1093/mnras/stv2235](https://doi.org/10.1093/mnras/stv2235)
- Pfeffer, J., Lardo, C., Bastian, N., Saracino, S., & Kamann, S. 2021, MNRAS, 500, 2514, doi: [10.1093/mnras/staa3407](https://doi.org/10.1093/mnras/staa3407)
- Pfister, H., Volonteri, M., Dubois, Y., Dotti, M., & Colpi, M. 2019, MNRAS, 486, 101, doi: [10.1093/mnras/stz822](https://doi.org/10.1093/mnras/stz822)
- Piatti, A. E., Mestre, M. F., Carballo-Bello, J. A., et al. 2021, A&A, 646, A176, doi: [10.1051/0004-6361/202040038](https://doi.org/10.1051/0004-6361/202040038)
- Plotkin, R. M., Gallo, E., & Jonker, P. G. 2013, ApJ, 773, 59, doi: [10.1088/0004-637X/773/1/59](https://doi.org/10.1088/0004-637X/773/1/59)
- Plotkin, R. M., Markoff, S., Kelly, B. C., KÖrding, E., & Anderson, S. F. 2012, MNRAS, 419, 267, doi: [10.1111/j.1365-2966.2011.19689.x](https://doi.org/10.1111/j.1365-2966.2011.19689.x)
- Prugniel, P., & Simien, F. 1997, A&A, 321, 111
- Putman, M. E., Gibson, B. K., Staveley-Smith, L., et al. 1998, Nature, 394, 752, doi: [10.1038/29466](https://doi.org/10.1038/29466)
- Read, J. I., Goerdt, T., Moore, B., et al. 2006, MNRAS, 373, 1451, doi: [10.1111/j.1365-2966.2006.11022.x](https://doi.org/10.1111/j.1365-2966.2006.11022.x)
- Ricarte, A., Tremmel, M., Natarajan, P., Zimmer, C., & Quinn, T. 2021, MNRAS, 503, 6098, doi: [10.1093/mnras/stab866](https://doi.org/10.1093/mnras/stab866)
- Riess, A. G., Macri, L. M., Hoffmann, S. L., et al. 2016, ApJ, 826, 56, doi: [10.3847/0004-637X/826/1/56](https://doi.org/10.3847/0004-637X/826/1/56)
- Roche, E. A. 1850, Montpellier Academy of Sciences and Letters. Mémoires de la section des sciences, 1, 333
- Saha, K., Graham, A. W., & Rodríguez-Herranz, I. 2018, ApJ, 852, 133, doi: [10.3847/1538-4357/aa9ed8](https://doi.org/10.3847/1538-4357/aa9ed8)
- Sahu, N., Graham, A. W., & Davis, B. L. 2019, ApJ, 876, 155, doi: [10.3847/1538-4357/ab0f32](https://doi.org/10.3847/1538-4357/ab0f32)
- Sánchez-Janssen, R., Côté, P., Ferrarese, L., et al. 2019, ApJ, 878, 18, doi: [10.3847/1538-4357/aaf4fd](https://doi.org/10.3847/1538-4357/aaf4fd)
- Sandage, A., Binggeli, B., & Tammann, G. A. 1985, AJ, 90, 1759, doi: [10.1086/113875](https://doi.org/10.1086/113875)
- Sandage, A., & Tammann, G. A. 1981, A Revised Shapley-Ames Catalog of Bright Galaxies (Washington, DC: Carnegie Institution)
- Savorgnan, G. A. D., Graham, A. W., Marconi, A., & Sani, E. 2016, ApJ, 817, 21, doi: [10.3847/0004-637X/817/1/21](https://doi.org/10.3847/0004-637X/817/1/21)
- Schlafly, E. F., & Finkbeiner, D. P. 2011, ApJ, 737, 103, doi: [10.1088/0004-637X/737/2/103](https://doi.org/10.1088/0004-637X/737/2/103)
- Scott, N., & Graham, A. W. 2013, ApJ, 763, 76, doi: [10.1088/0004-637X/763/2/76](https://doi.org/10.1088/0004-637X/763/2/76)
- Sérsic, J. L. 1963, Boletín de la Asociación Argentina de Astronomía La Plata Argentina, 6, 41
- Shipp, N., Drlica-Wagner, A., Balbinot, E., et al. 2018, ApJ, 862, 114, doi: [10.3847/1538-4357/aacdab](https://doi.org/10.3847/1538-4357/aacdab)
- Sivakoff, G. R., Jordán, A., Sarazin, C. L., et al. 2007, ApJ, 660, 1246, doi: [10.1086/513094](https://doi.org/10.1086/513094)

- Soria, R., Hau, G. K. T., Graham, A. W., et al. 2010, MNRAS, 405, 870, doi: [10.1111/j.1365-2966.2010.16517.x](https://doi.org/10.1111/j.1365-2966.2010.16517.x)
- Soria, R., Kolehmainen, M., Graham, A. W., et al. 2021, MNRAS, submitted
- Soria, R., Long, K. S., Blair, W. P., et al. 2014, Science, 343, 1330, doi: [10.1126/science.1248759](https://doi.org/10.1126/science.1248759)
- Soria, R., & Motch, C. 2004, A&A, 422, 915, doi: [10.1051/0004-6361:20040265](https://doi.org/10.1051/0004-6361:20040265)
- Spitzer, Lyman, J., & Baade, W. 1951, ApJ, 113, 413, doi: [10.1086/145406](https://doi.org/10.1086/145406)
- Strader, J., Chomiuk, L., Maccarone, T. J., et al. 2012, ApJL, 750, L27, doi: [10.1088/2041-8205/750/2/L27](https://doi.org/10.1088/2041-8205/750/2/L27)
- Sunyaev, R. A., Tinsley, B. M., & Meier, D. L. 1978, Comments on Astrophysics, 7, 183
- Sutton, A. D., Roberts, T. P., Walton, D. J., Gladstone, J. C., & Scott, A. E. 2012, MNRAS, 423, 1154, doi: [10.1111/j.1365-2966.2012.20944.x](https://doi.org/10.1111/j.1365-2966.2012.20944.x)
- Takekawa, S., Oka, T., Iwata, Y., Tsujimoto, S., & Nomura, M. 2020, ApJ, 890, 167, doi: [10.3847/1538-4357/ab6ff6](https://doi.org/10.3847/1538-4357/ab6ff6)
- Terzić, B., & Graham, A. W. 2005, MNRAS, 362, 197, doi: [10.1111/j.1365-2966.2005.09269.x](https://doi.org/10.1111/j.1365-2966.2005.09269.x)
- Terzić, B., & Sprague, B. J. 2007, MNRAS, 377, 855, doi: [10.1111/j.1365-2966.2007.11655.x](https://doi.org/10.1111/j.1365-2966.2007.11655.x)
- Thomas, G. F., Jensen, J., McConnachie, A., et al. 2020, ApJ, 902, 89, doi: [10.3847/1538-4357/abb6f7](https://doi.org/10.3847/1538-4357/abb6f7)
- Tody, D. 1986, in Society of Photo-Optical Instrumentation Engineers (SPIE) Conference Series, Vol. 627, Instrumentation in astronomy VI, ed. D. L. Crawford, 733, doi: [10.1117/12.968154](https://doi.org/10.1117/12.968154)
- Tody, D. 1993, in Astronomical Society of the Pacific Conference Series, Vol. 52, Astronomical Data Analysis Software and Systems II, ed. R. J. Hanisch, R. J. V. Brissenden, & J. Barnes, 173
- Tonry, J. L. 1985, AJ, 90, 2431, doi: [10.1086/113948](https://doi.org/10.1086/113948)
- Tremaine, S. D., Ostriker, J. P., & Spitzer, L., J. 1975, ApJ, 196, 407, doi: [10.1086/153422](https://doi.org/10.1086/153422)
- Tremmel, M., Governato, F., Volonteri, M., Pontzen, A., & Quinn, T. R. 2018, ApJL, 857, L22, doi: [10.3847/2041-8213/aabc0a](https://doi.org/10.3847/2041-8213/aabc0a)
- Tremou, E., Strader, J., Chomiuk, L., et al. 2018, ApJ, 862, 16, doi: [10.3847/1538-4357/aac9b9](https://doi.org/10.3847/1538-4357/aac9b9)
- Tully, R. B., & Fisher, J. R. 1977, A&A, 500, 105
- Velazquez, H., & White, S. D. M. 1999, MNRAS, 304, 254, doi: [10.1046/j.1365-8711.1999.02354.x](https://doi.org/10.1046/j.1365-8711.1999.02354.x)
- Vorontsov-Vel'Yaminov, B. A. 1959, Atlas and Catalog of Interacting Galaxies, Vol. 1, 1959, 1
- Vorontsov-Velyaminov, B. A. 1977, A&AS, 28, 1
- Ward, C., Gezari, S., Frederick, S., et al. 2021, ApJ, 913, 102, doi: [10.3847/1538-4357/abf246](https://doi.org/10.3847/1538-4357/abf246)
- Webb, N. A., Guérou, A., Ciambur, B., et al. 2017, A&A, 602, A103, doi: [10.1051/0004-6361/201630042](https://doi.org/10.1051/0004-6361/201630042)
- Weinzirl, T., Jogee, S., Khochfar, S., Burkert, A., & Kormendy, J. 2009, ApJ, 696, 411, doi: [10.1088/0004-637X/696/1/411](https://doi.org/10.1088/0004-637X/696/1/411)
- Willmer, C. N. A. 2018, ApJS, 236, 47, doi: [10.3847/1538-4365/aabfdf](https://doi.org/10.3847/1538-4365/aabfdf)
- Woody, T., & Schlafman, K. C. 2021, AJ, 162, 42, doi: [10.3847/1538-3881/abff5f](https://doi.org/10.3847/1538-3881/abff5f)
- Yang, Q.-X., Xie, F.-G., Yuan, F., et al. 2015, MNRAS, 447, 1692, doi: [10.1093/mnras/stu2571](https://doi.org/10.1093/mnras/stu2571)
- Younes, G., Porquet, D., Sabra, B., & Reeves, J. N. 2011, A&A, 530, A149, doi: [10.1051/0004-6361/201116806](https://doi.org/10.1051/0004-6361/201116806)
- Yuan, Z., Chang, J., Beers, T. C., & Huang, Y. 2020, ApJL, 898, L37, doi: [10.3847/2041-8213/aba49f](https://doi.org/10.3847/2041-8213/aba49f)
- Zinnecker, H., Keable, C. J., Dunlop, J. S., Cannon, R. D., & Griffiths, W. K. 1988, in IAU Symposium, Vol. 126, The Harlow-Shapley Symposium on Globular Cluster Systems in Galaxies, ed. J. E. Grindlay & A. G. D. Philip (Dordrecht: Kluwer), 603
- Zoccali, M., Valenti, E., & Gonzalez, O. A. 2018, A&A, 618, A147, doi: [10.1051/0004-6361/201833147](https://doi.org/10.1051/0004-6361/201833147)
- Zocchi, A., Gieles, M., & Hénault-Brunet, V. 2019, MNRAS, 482, 4713, doi: [10.1093/mnras/sty1508](https://doi.org/10.1093/mnras/sty1508)